Thermoelectric property of doped $LiNbO_2$

Thesis submitted in partial fulfillment of the requirements

for the degree of Master of Philosophy in Physics

Quaid-i-Azam University Islamabad

by

Riaz Ahmad

Department of Physics

Quaid-i-Azam University Islamabad

Pakistan

Feb. (2018)

CERTIFICATE

This is to certify that **Mr. Riaz Ahmad** has submitted a dissertation on "Thermoelectric property of doped $LiNbO_2$", as a partial fulfillment of the requirements for the award of M. Phil. degree in physics. It is also affirmed that, the dissertation submitted by him is original, bona-fide and genuine.

Assoc. Prof. Dr. Gul Rahman
(Supervisor)

Prof. Dr. Arif Mumtaz
(Chairman)

Dedication

Dedicated to my beloved parents and respected teachers who are the nation builders

Acknowledgements

First of all I would like to convey my profound and cordial gratitude to my supervisor and true inspiration to the field ***Dr. Gul Rahman***, whose polite and kind behavior, generous suggestions, cooperation, encouragement and advises were greatly useful in completing this crucial task. I am extremely thankful to all my academic teachers.

I am also very thankful to GIKI Pakistan's support for providing their cluster, that have helped me achieve this milestone.

Then I would like to thank my family, who are the most important part of my life. I would like to thank my parents for their support and love throughout my life. I am also thankful to my siblings for their support and prayers.

I gratefully acknowledge the invaluable suggestions and generous guidance of my senior Mr. Altaf Ur Rahman. I am really thankful to my research colleagues Asad Ali, Saima and Ahmad Ali for their suggestions and prolific discussions.

I can't imagine completing my acknowledgement without considering my friend Sadiq Ullah, Mazhar Iqbal and hostel roommate M. Waleed Ahmed. I really enjoyed their company from beginning to end.

Abstract

Using first-principles calculations, we investigated the electronic and thermoelectric (TE) properties of doped $LiNbO_2$. We show that $LiNbO_2$ is a direct bandgap material and the bonding between Nb and O atoms is covalent. Seebeck coefficient, electrical conductivity, power factor, and figure of merit of $LiNbO_2$ are optimized under electron and hole carrier concentrations, using the Boltzman transport theory. Electron carrier concentrations can give larger figure of merit. The effect of O and Li vacancies on the electronic and TE properties are also studied, and we show that Li (O) vacancy in $LiNbO_2$ generates holes (electrons). Though n-type $LiNbO_2$ is expected to have superior TE proprieties over p-type $LiNbO_2$, but the defect formation energy of O vacancy is larger than the Li vacancy in $LiNbO_2$. The electronic structures and TE properties of $Li_{1-x}A_xNbO_2$(A=Ta,Ni) and $LiNb_{1-x}Ta_xO_2$ (x=0.0625) as a function of temperature are also investigated. Doping of Ta at Nb site is energetically more favourable as compared with Ni doping in $LiNbO_2$. Hence, we believe that Nb-doped $LiNbO_2$ could be a possible candidate material for thermoelectric applications. Our calculations also agree with the available experimental TE data of $LiNbO_2$.

Contents

List of Figures

List of Tables

Chapter 1

Introduction

1.1 Thermoelectricity

In the present age we are facing energy crises and we have one of the critical current issues to find alternative energy sources without having bad effects on our environment. We have many cheap as well expensive energy sources but they are very harmful for the environment, like fossil fuels etc. Thermoelectric effect is known one of the best alternative source for power generation, the effect can be achieved through thermoelectric material to overcome the energy crises [1]. Thermoelectric effect is the effect in which direct conversion of temperature difference and electrical energy is described. Thermoelectric materials directly convert thermal energy to electricity when a temperature gradient is formed on thermoelectric junctions. Similarly in converse case, temperature difference will be observed if voltage is applied to a thermoelectric material. This effect can be used to generate electricity and to control the temperature of the material. The efficiency of the thermoelectric materials depend on the dimensionless figure of merit ZT [2].

$$ZT = \frac{\mathcal{S}^2\sigma}{\kappa}T \tag{1.1}$$

These terms will be explained later but here $\sigma, \mathcal{S}, \kappa$ are the electrical conductivity, Seebeck coefficient and thermal conductivity respectively. Thermoelectric effect can be described in three different methods.

1) Seebeck effect(2) Peltier effect and (3) Thomson effect

1.2 Seebeck effect

Seebeck was the name of a German physicist, full name Thomas Johann Seebeck(9 April 1770– December 10, 1831).He observed the first thermoelectric effect in the Berlin Academy of Sciences on December, 1820 [3]. He joined the end of two different wires, copper and bismuth to form a loop, by heating one end of the loop and he observed voltage was developed in the circuit. The metal wires were known as a thermocouple from which the circuit was formed. This effect is due to the conversion of thermal energy to electrical energy.

Conversion of temperature difference to electricity is called Seebeck effect. Seebeck observed during his experiment that a compass needle deflects by forming a close loop from two different metal wires, having a temperature difference between the junctions of those wires. This temperature difference creates current in the loop. Seebeck initially did not recognize it, he believed that it was due to the magnetism induced by the temperature's difference and thus he called it thermo-magnetic effect.

A Danish physicist H. C. Orsted later on recognized , it is an electrical current

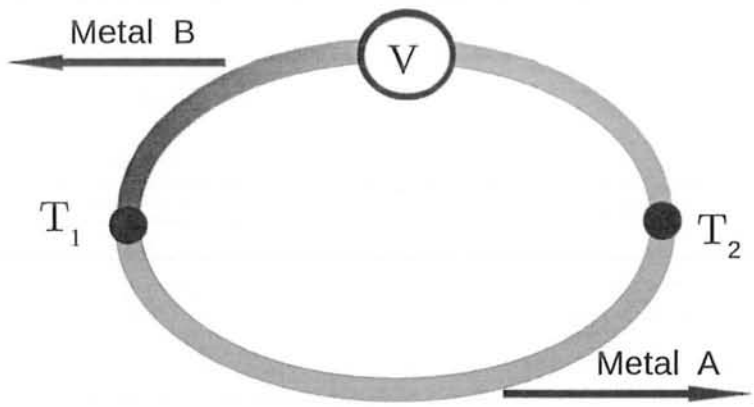

Figure 1.1: Circuit diagram for Seebeck Effect with two different metal wires having different temperature at both junctions T_1 at low temperature, T_2 at high temperature

which according to Ampere's law deflects the magnet. So due to thermal energy the valance electrons moves from high energy level to lower energy level. It will move from warmer end to the cold end.

At cold side Fermi distribution is sharp while on hot side Fermi distribution is soft i.e., the higher concentration of electrons above the Fermi energy on hot side, while fewer electrons above the Fermi energy on cold side. The electrons at hotter end have higher kinetic energy as compared to colder end and has a tendency to move towards colder end and the movement of electrons generate electric current. This current or electrical energy, which is generated due to this temperature difference is very small in magnitude though. The relation between temperature and voltage can be observed as

$$S = \frac{\Delta V}{\Delta T} \tag{1.2}$$

Where S is the Seebeck coefficient which is also known as thermopower, and is equal to the ratio of voltage difference to temperature difference. Its value may be negative or positive depending upon on the majority carrier, whether they are electrons or holes. Though SI unit of Seebeck coefficient is V/K but usually it gives very small value so its is measure in $\mu V/K$.

1.3 Peltier and Thomson effect

This is another method or effect through which thermoelectric effect can be described. Jean Charles Athanase Peltier(February 22, 1785 – October 27, 1845), was a french physicist, he was the author of many papers in the different areas of physics but he is very well known for thermoelectric effect. In 1834 Peltier was observing Seebeck effect and he realized that the converse of this effect can also be possible. He discovered that electric current in two different metals will produce heat or cold depending on the direction of current [4]. In other words, this is the effect in which a temperature difference is created by applying a voltage between two electrodes. This effect is even stronger for different semiconductors. This effect may be consider as the inverse of Seebeck effect in which conversion of heat to electricity was observed. Here heat may be generated or absorbed within each end of a material due to current across that material.

William Thomson also known as Lord Kelvin (26 June 1824–December 17,1907), who was a mathematical physicist and engineer, almost twenty years after Peltier

effect in 1851 observed the relation between Seebeck and Peltier effect. He described and issued a comprehensive explanation on Seebeck and Peltier effect and interrelation between them,and now known as Thomson effect [?]. The coefficient of these effects are related through thermodynamics. Thomson effect describes heating or cooling of a material with temperature. It states that if current density is passed in a conductor it will produce heat rate per unit volume as

$$q = kJ\Delta T \tag{1.3}$$

Where k Thomson coefficient, J current density and ΔT is the temperature difference. This effect produce in a single material not in two different material. So heat will be absorbed or produced when current flows in a material with a temperature gradient. The amount of heat produced is directly related to both current density and temperature gradient or electric current will be generated in a material if the flow of heat produce a temperature gradient in that material.
Thomson coefficient has two different relations, according to first relation
if we let $\alpha - \beta = \gamma$ in Peltier effect then

$$k = \frac{d\gamma}{dT} - S \tag{1.4}$$

Where k is Thomson coefficient, T is absolute temperature and S, γ are Seebeck and Peltier coefficient respectively. While Thomson second relation is

$$\gamma = TS \tag{1.5}$$

Putting equation 1.6 in 1.5 we get

$$k = T\frac{dS}{dT} \tag{1.6}$$

equation 1.6 shows a direct relation between Seebeck and Peltier coefficients. Which leads to another relation for Thomson coefficient in the form of equation 1.6.

1.4 Thermoelectric efficiency

Thermoelectric devices offer the promise of power generation and also includes in their applications, the refrigeration which might be very useful in some cases and the most important and interesting fact is that it is very friendly to the environment. As a temperature difference across a material will produce a voltage difference which can be used to provide power. In the same material one end of the material can be cool for refrigeration purpose using current. It is a promising challenge in the study of thermoelectricity to find such materials which can provide power generation and refrigeration at higher efficiency which is more efficient and less pollutant phenomena. The efficiency of such materials can be determined through the dimensionless figure of merit ZT [2].

$$ZT = \frac{S^2\sigma}{\kappa}T$$

Figure of merit is divided into two parts, the Seebeck coefficient's square and electrical conductivity both combined are consider as power factor(PF=σ S^2) and the second part is thermal conductivity, while thermal conductivity has also two parts lattice thermal conductivity and electron thermal conductivity. In this equation the power factor is directly related to efficiency and thermal conductivity is inversely related so according to these two parts the efficiency will be maximum if power factor is larger and thermal conductivity is smaller. Materials having figure of merit

greater than unity are consider very good thermoelectric materials for power generation, there are very few materials which has ZT greater than one, like $BaTiO_3$ and $CoSb_3$ [5,6]. Similarly $NaCoO_2$ and BiCuTeO are also considered best thermoelectric materials with layered structure [7,8]. Scientist are searching for such type of materials that has higher efficiency. How the behavior of different parameters in ZT for different types of materials vary shown in Fig. 1.2 [9]

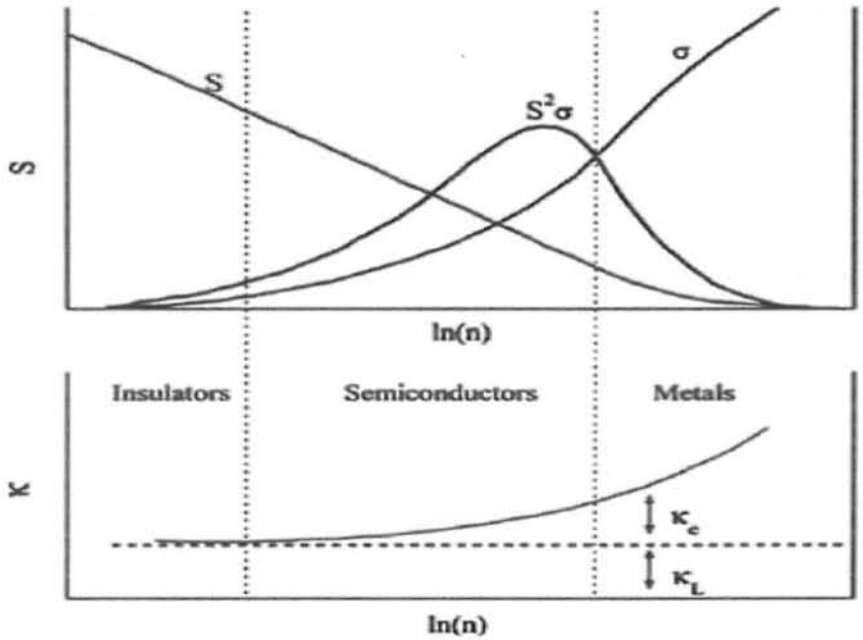

Figure 1.2: The effect of electrical conductivity, thermal conductivity and Seebeck coefficient with carrier concentration [9].

From Fig. 1.2 we can see that all the parameters are inter related to each other, improving ZT we are facing the difficulties, if we increase S (Seebeck) it leads to direct decrease σ (electrical conductivity), on the other hand increasing σ leads to increasing thermal conductivity (k_e) as we know it from the Wiedemann-Franz law. The maximum PF in Semiconductor occurs around $10^{19}/\text{cm}^3$ carrier concentration.

Comparing ZT for in these three different regions, we can conclude that semi conductors are the best material for thermoelectric phenomena as they show larger efficiency as compared to insulators and metals. The point should be noted here for lattice thermal conductivity which is kept constant for all types of material because we only deal with electron thermal conductivity in our calculation.

1.5 Seebeck coefficient

Seebeck coefficient has an important role in the efficiency of a material, larger the value of Seebeck coefficient and smaller thermal conductivity leads to a good thermoelectric material. This coefficient is discussed in above section, its behavior is different in different material, like semiconductors and metals. The mechanism is quite different in semiconductors and metals for the generation of Seebeck effect, in fact if we look into a metal we know that its Fermi level and carrier concentrations do not change relatively with temperature. But carriers on one end of a semiconductor has different energy. Thermal energy of hot end carriers will be more from the cold end carriers, diffusion will start from hot to cold end. Opposite electric field is formed in the cold end due to more localized carriers. So the rate of diffusion, moving hot carriers to cold end and rate at which cold carriers moving to hot end due to electric field will be balanced and hence equilibrium is reached. As a result the voltage difference will form with a temperature gradient, which is called Seebeck voltage, Seebeck voltage per unit temperature gradient is known as Seebeck coefficient S. If we want larger S we can add only one type of carrier like electrons or holes, adding both will weaken the voltage due to the excess of both carriers in the

cold end. The Mott equation for enhansing S through electronic DOS is related as

$$S = \frac{\pi^2}{3}\frac{k_B^2 T}{e}\frac{\mathrm{d}}{\mathrm{d}E}\ln\left[\sigma(E)\right]\Big|_{E=E_F} \tag{1.7}$$

Where $e, \sigma(E)$ and k_B are charge of an electron, electrical conductivity and Boltzmann's constant respectively.

The expression for Seebeck can be written using Pisarenko relation [10].

$$S = \frac{8\pi^2 k_B^2}{3eh^2}\left(\frac{\pi}{3n}\right)^{\frac{2}{3}} m^* T \tag{1.8}$$

Where n is carrier concentration, k_B is Boltzmann constant, h is Plank's constant, T is absolute temperature and m^* is the effective mass of the carrier. According to this relation, S is directly related to effective mass and inversely proportional to carrier concentration. Typically Seebeck coefficient of metals is small due to half-filled bands which is caused by equal and opposite charges, which cancel each other when contributing to thermoelectric voltage. However, large Seebeck was observed in alloys and "heavy fermion" systems or solid solution of rare-earth elements. Best thermoelectric materials are typically doped semiconductors with carrier concentration between 10^{19} to 10^{21} carriers per cm^3 [11].

1.6 Electrical conductivity

Electrical conductivity is another important parameter of power factor as well of figure of merit, it is denoted as σ and it is the ability of a material to let charge carriers passes through its crystal lattice. This idea can be represented through a mathematical expression as under [9].

$$\sigma = e\mu n \tag{1.9}$$

Where μ is carrier mobility, n is charge carrier density

$$\mu = \frac{\tau e}{m^*} \tag{1.10}$$

is directly related to relaxation or scattering time (τ) and inversely linked with carrier effective mass(m^*). It also depends on the drift velocity that is determined by scattering time (τ), it means that for how long the carrier are accelerated by electric field until it collides and changes its energy or direction. What are the sources of scattering? Scattering in semiconductors are due to neutral impurities, electron-phonon interaction, ionized impurities and electron-electron interaction [12]. Due to unionized donors in semiconductors at low temperature scattering become dominant, because at low temperature carriers freeze out at the impurity. Formally mobility is independent of temperature but in some experiments it shows a weak dependence for semiconductors. At very high carrier concentrations neutral impurity scattering is strong for example above 10^{19} /cm^3.

In electron-phonon scattering, due to acoustic wave the change occur in atomic spacing which results change in energy band gap on the atomic scale. The mobility is related to temperature due to this deformation potential as $\mu \propto T^{\frac{-3}{2}}$ while the mobility is related to temperature due to piezoelectric scattering as $T^{\frac{-1}{2}}$.

1.7 Thermal conductivity

Thermal conductivity has much importance as power factor do in figure of merit. It is represented as κ, which also consist of two parts, i.e., $\kappa = \kappa_e + \kappa_l$ while κ_e and κ_l are electron thermal conductivity and lattice thermal conductivity, respectively. κ_e represents heat transportation due to moving charge carriers. Wiedemann-Franz presented a law for metals and semiconductors with narrow band-gap, which states

that the ratio of thermal to electrical conductivity of a metal is proportional to temperature, mathematically

$$\kappa_e = LT\sigma \tag{1.11}$$

Where σ is electrical conductivity, T is temperature and L is Lorenz number, which is derived by Sommerfeld for metals and heavily doped semiconductors [13].

Considering only σ, the Wiedemann-Franz's law gives a suitable approximation to the electronic part.

Where κ_l is the lattice contribution to thermal conductivity due to to lattice vibration or phonons, from the kinetic theory of gases

$$\kappa_l = l\frac{v_s C_v}{3} \tag{1.12}$$

l represents the mean free phonon path, C_v is the specific heat at constant volume and v_s is the speed of sound. We know from Debye model C_v is directly related to T^3 at low temperature when temperature is less than Debye temperature and $C_v = 3R$, at higher temperature ($T >>$ Debye temperature), where R is ideal gas constant. It implies that κ_l basically depends on l which is determined by phonon-phonon scattering. Looking to all these parameters and all conditions, we need small thermal conductivity and large power factor, thus we can achieve high figure of merit.

1.8 Introduction to $LiNbO_2$

Transition metal oxides with lithium intercalation are considered very important material for the advancement of energy storage technologies. Lithium can easily be replaced and can be removed from the layered crystal structure of Lithium intercalated transition metal oxide material. Although a minor lattice phase change occur

with the removal of lithium, but no major phase change occur, even for example if 50% of lithium is reversibly removed from $LiCoO_2$ [14]. $LiNbO_3$, $LiNbO_2$, $LiCoO_2$, etc., are lithium intercalated layered transition metal oxides. Some of these type of compounds got full attention but $LiNbO_2$ has been minimally investigated.
$LiNbO_2$ is known as lithium niobite. Lithium niobite is the suboxide of $LiNbO_3$. It has the same layered structure like $LiCoO_2$, but with different space group. $LiNbO_2$

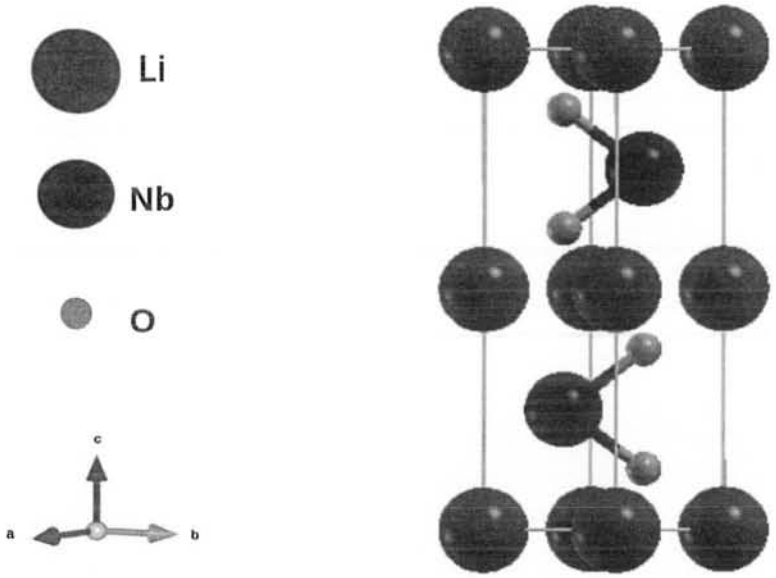

Figure 1.3: Crystal structure of $LiNbO_2$, red, blue and green colors corresponds to Lithium, Niobium and oxygen atom respectively.

has $P6_3$ /mmc space group(No. 194). It has hexagonal layered crystal structure with Li atom plane sandwiched between Nbo_2 layer [15]. Its unit cell consist of 8 atoms, with two Li, two Nb and four O atoms. Different values of lattice parameters were observed e.g, a=2.90Å, c=10.46Å in reference [16], a=2.912Å, c=10.46Å in reference [15], a=2.908Å, c=10.441Å in reference [19]. $LiNbO_2$ is a direct band

gap semiconductor given by Novikov *et al* [17], while there is some disagreement about the band gap of $LiNbO_2$ in literature, e.g, a band gap of 1.5 eV was reported by Novikov *et al.* [17], while 2 eV band gap was also reported from Geselbracht *et al.* [18]. X-ray diffraction study shows superconductivity in $Li_{1-x}NbO_2$ at 5.5K due to small distortion in crystal structure [19].

For power generation applications thermoelectric materials got increasing attention and interest, $LiNbO_2$ is also investigated for this purpose. Jamil and his coworker synthesis and find the thermoelectric properties of p-type $Li_{1-x}NbO_2$ compound [20]. Synthesis was carried through solid state reaction process under reduce atmosphere. The crystal structure was characterized through XRD (x-ray diffraction) method, they observed the hexagonal structure of $LiNbO_2$ but the structure was observed to be distorted after creating Lithium vacancy through solid state reaction. For small amount of Li vacancy the lattice parameters a and c were decreasing and increasing respectively while for high lithium vacancy the case was inverse. As a is the metal-metal distance of NbO layer, so they concluded that the evaluation of Nb oxidation state causes decrease in ionic radii and hence in lattice parameter a. They also suggest that due to Lithium vacancy the attractive force becomes weak between sheets and alkaline ions, which causes increase in lattice parameter c. While low thermal conductivity was observed at x=0.1 and x=0.2 in $Li_{1-x}NbO_2$. The efficiency is the combine effect of power factor and thermal conductivity, and we know that power factor which is the product of electrical conductivity and Seebeck coefficient's square is directly related to figure of merit of efficiency, and thermal conductivity is inversely linked to figure of merit. So power factor must be higher and thermal conductivity must be smaller as much as possible. The figure of merit from their work is mentioned here

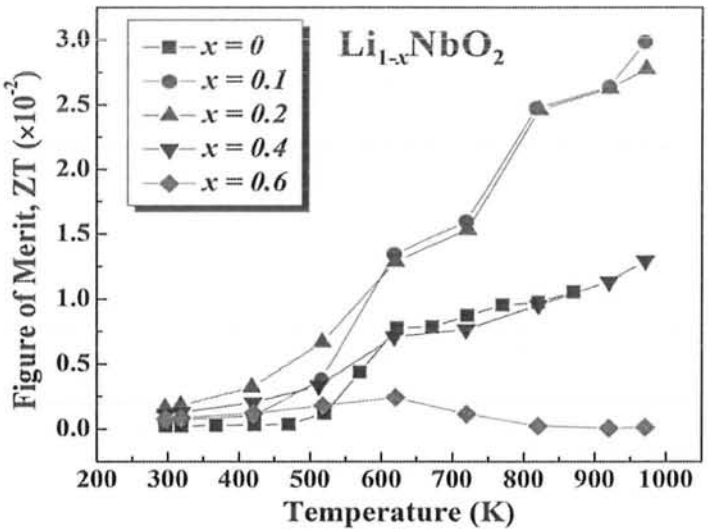

Figure 1.4: Figure of merit on y-axis for $Li_{1-x}NbO_2$ with different x values corresponding to Lithium vacancy, with temperature on x-axis [20].

In Figure 1.4 ZT is higher for small amount of Lithium vacancy but for higher vacancy the electrical conductivity and Seebeck coefficient were reduced and thermal conductivity was increased which causes decrease in figure of merit. The figure of merit can be improved with more modifications and different changes in $LiNbO_2$. Researchers are working on this compound with different options and advancement to get more useful advantages from it. We also tried to add our contribution to this cause, we first simply add carrier concentration like holes and electrons to $LiNbO_2$ and looked for band structure and thermoelectric parameters, then we take the $2 \times 2 \times 2$ super cell of $LiNbO_2$ and looked for the same, similarly we add some impurities to different positions and made some defects like Lithium vacancy and Oxygen vacancy and observed the band structure and thermoelectric parameters.

Chapter 2

Method of Calculation

2.1 Theoretical Background

Many body problem in solids is considered to be unsolvable problem analytically, but there are several approximation and computational methods for this type of problems, which can give a good approximation to these types of problems. Density functional theory is also a method for approximate solution to many body problems. This method is the solution to Shrödinger's many body equation as a functional of charge density. Shrödinger's equation [21]

$$\hat{\mathbf{H}}\Psi = E\Psi \tag{2.1}$$

Where $\hat{\mathbf{H}}$ is Hamiltonian operator, which is the sum of kinetic and potential energies, Ψ is the wave function and E is the total energy of the system. The solution to this equation gives us total energy of the system and all wanted properties which is essential in Quantum Mechanics. In case of density functional theory, energy is required as a functional of density. Where

$$\rho(\mathbf{r}) = |\Psi|^2$$

is the density as a function of $\mathbf{r}$.

For many body system with N electrons, k nuclei and Z_n charges the Hamiltonian is written as [22]

$$\begin{aligned}\hat{\mathbf{H}} = \sum_{i=1}^{N} \frac{\mathbf{P}_i{}^2}{2m} + \sum_{n=1}^{k} \frac{\mathbf{P}_n{}^2}{2M_n} + \frac{1}{4\pi\varepsilon_0}\frac{1}{2}\sum_{i=1;j>i}^{N} \frac{e^2}{|\mathbf{r}_i - \mathbf{r}_j|} - \\ \frac{1}{4\pi\varepsilon_0}\sum_{n=1}^{k}\sum_{i=1}^{N} \frac{Z_n e^2}{|\mathbf{r}_i - \mathbf{R}_n|} + \frac{1}{4\pi\varepsilon_0}\frac{1}{2}\sum_{n=1;n\neq t}^{k} \frac{Z_n Z_t e^2}{|\mathbf{R}_n - \mathbf{R}_t|}\end{aligned} \tag{2.2}$$

Where the first and second terms in the above equation are the kinetic energies of electrons and nuclei respectively having m mass of the electron and M mass of the nuclei, the next term, 3rd term is the Coulomb repulsion between electrons, the second last term represents the attraction between electrons and nuclei, while the last term is the Coulomb repulsion between nuclei, and the index i, n in the equation are used for electrons and nuclei, respectively. This Hamiltonian looks very complicated which depends upon the position vector $\mathbf{r}_i$ and $\mathbf{R}_n$ of the electrons and nuclei respectively.

2.2 Born–Oppenheimer Approximation

In the above Hamiltonian if the number of electrons and nuclei are not smaller, then it is impossible to solve the Shrödinger's equation directly even with the help of a larger and faster computer. Some important approximations are required to solve Shrödinger's many body equation, the first step to these approximation is separating the degrees of freedom of motion of the nuclei from those of the electrons because the nuclei are very heavier and their motion can be neglected as compared to those of electrons. So electrons and ions can be treated separately for electrons ions can

considered as fixed. This approximation was first made by Born–Oppenheimer, and known as Born–Oppenheimer approximation [22]. From this approximation if we drop the kinetic energy term and ion-ion interaction term in the above equation, it can be written as

$$\hat{\mathbf{H}}_{BO} = \sum_{i=1}^{N} \frac{\mathbf{P}_i{}^2}{2m} + \frac{1}{4\pi\varepsilon_0}\frac{1}{2}\sum_{i=1;j>i}^{N} \frac{e^2}{|\mathbf{r}_i - \mathbf{r}_j|} - \frac{1}{4\pi\varepsilon_0}\sum_{n=1}^{k}\sum_{i=1}^{N} \frac{Z_n e^2}{|\mathbf{r}_i - \mathbf{R}_n|} \tag{2.3}$$

If we denote the interaction term (ion, electron attraction term) by $V_{ext}(\mathbf{r}_i)$ and take the constant used in the equation equal to unity, which are Hartree atomic units, the above Hamiltonian after simplification can be written as

$$\hat{\mathbf{H}}_{BO} = -\frac{1}{2}\sum_{i} \nabla_i{}^2 + \sum_{i=1}\sum_{j>i} \frac{1}{|\mathbf{r}_i - \mathbf{r}_j|} + \sum_{i} V_{ext}(\mathbf{r}_i) \tag{2.4}$$

After this approximation the solution to many body problem is still very difficult for more than few electrons, after which many theories and approximations were made by different scientists.

2.3 Hohenberg-Kohn Theorem

Hohenberg and Kohn presented their theorem in 1964 [23] they proved that $V_{ext}(\mathbf{r}_i)$ can be uniquely determined by the electron ground state density $\rho_o(\mathbf{r})$ and the energy can be written as functional of electron density that can be minimized by ground state. Hohenberg and Kohn proved their theorem on a contradiction based, they supposed two different systems having the same electron density and proved it wrong. Let these two different systems have different external potentials, Hamiltonians and different energies but they have the same charge density

$$V_{1ext}(\mathbf{r}_i), \hat{\mathbf{H}}_1 \text{ and } \rho_o(\mathbf{r})$$

while system two has

$$V_{2ext}(\mathbf{r}_i), \hat{\mathbf{H}}_2 \text{ and } \rho_o(\mathbf{r})$$

let E_1, E_2 be the ground state energies of $\hat{\mathbf{H}}_1$ and $\hat{\mathbf{H}}_2$ respectively where

$$\hat{\mathbf{H}}_1 = T_e + V_{ee} + V_{1ext}(\mathbf{r}_i)$$

and

$$\hat{\mathbf{H}}_2 = T_e + V_{ee} + V_{2ext}(\mathbf{r}_i)$$

where T_e, V_{ee} are the electrons Kinetic and Potential energy terms.

from variational principle

$$E_1 < \langle \Psi | \hat{\mathbf{H}}_1 | \Psi \rangle \tag{2.5}$$

$$E_1 < \langle \Psi | \hat{\mathbf{H}}_1 + \hat{\mathbf{H}}_2 - \hat{\mathbf{H}}_2 | \Psi \rangle$$

$$E_1 < \langle \Psi | \hat{\mathbf{H}}_2 | \Psi \rangle + \langle \Psi | \hat{\mathbf{H}}_1 - \hat{\mathbf{H}}_2 | \Psi \rangle$$

$$E_1 < E_2 + \int \rho_o(\mathbf{r})[V_{1ext}(\mathbf{r}_i) - V_{2ext}(\mathbf{r}_i)]d\mathbf{r} \tag{2.6}$$

similarly for E_2 we have

$$E_2 < \langle \Psi | \hat{\mathbf{H}}_2 | \Psi \rangle \tag{2.7}$$

$E_2 < \langle \Psi | \hat{\mathbf{H}}_2 + \hat{\mathbf{H}}_1 - \hat{\mathbf{H}}_1 | \Psi \rangle$

$$E_2 < \langle \Psi | \hat{\mathbf{H}}_1 | \Psi \rangle + \langle \Psi | \hat{\mathbf{H}}_2 - \hat{\mathbf{H}}_1 | \Psi \rangle$$

$$E_2 < E_1 - \int \rho_o(\mathbf{r})[V_{1ext}(\mathbf{r}_i) - V_{2ext}(\mathbf{r}_i)]d\mathbf{r} \tag{2.8}$$

adding equation 1.6 and 1.8 we get

$$E_1 + E_2 < E_1 + E_2$$

Which is not possible, so there can't be two different $V_{cxt}(\mathbf{r}_i)$ that gives the same ground state density.

Similarly variational principle can be used for the ground state energy [24]. According to this principle the ground state energy can be written as

$$E_0 = \frac{\langle \Psi | \hat{\mathbf{H}} | \Psi \rangle}{\langle \Psi | \Psi \rangle} \tag{2.9}$$

for normalized wave function we have

$$\langle \Psi | \Psi \rangle = 1$$

$$E_0[\rho] = min_{[\rho]} \Big\langle \Psi | \hat{\mathbf{H}} | \Psi \Big\rangle = min_{[\rho]} \left[F[\rho] + \int \rho[\mathbf{r}] V_{ext}[\rho(\mathbf{r})] d\mathbf{r} \right] \tag{2.10}$$

Where Ψ is the total wave function or a functional of the density $[\rho]$, $F[\rho]$ is the term used for all internal energies like kinetic and potential energies also known as universal functional, while V_{ext} is the potential specifically external potential which is due to ions. It was a good approach to utilize the minimum energy or the ground state energy, but the problem is still there, how to get the many particle system wave function or the density functional. The minimum ground state energy can be described by variational method iteration, to go further with this problem we need the Kohn-Sham work.

2.4 Kohn-Sham theory

After Hohenberg-Kohn's theorem, in 1965 Kohn and Sham proposed an idea based on Hohnberg Kohn theorem, they replaced the many body interacting system by an auxiliary non interacting system.This idea is known as Kohn-Sham insatz [25]. In this theorem the interaction electron system will be replaced with a non-interacting

electron system having the same ground state density(ρ). The density of that non interacting system can be written as

$$\rho(\mathbf{r}) = \int_i^N \psi_i^*(\mathbf{r})\psi_i(\mathbf{r})d\mathbf{r} = \sum_i |\psi_i(\mathbf{r})|^2 \tag{2.11}$$

ψ_i is the noninteracting orbital wave function which gives the electron charge density $\rho(\mathbf{r})$, where N represents the number of occupied orbitals. The energy functional in the Hohnberg-Kohn theorem can be rearranged as

$$E_{KS}[\rho] = T_0[\rho] + E_H[\rho] + \int \rho[\mathbf{r}]V_{ext}[\rho]d\mathbf{r} + E_{xc}[\rho] \tag{2.12}$$

The last term is new here which is known as exchange correlation term, it include all those terms which were missing using the independent electron orbital system instead of full many electron interacting system. The first term is the kinetic energy term for the non interacting system of electrons, the second term is known as Hatree energy term or also known as mean-field approximation and it states that each electron observe or feels average effect from those all electrons in that system, and can be written as

$$E_H(\rho) = \tfrac{1}{2}\int\int \tfrac{\rho(\mathbf{r})\rho(\mathbf{r}')}{|\mathbf{r}-\mathbf{r}'|}\, d\mathbf{r}d\mathbf{r}'$$

Where the third term in equation(2.12) is the interaction term recognized as interacting term with ions also known as external energy term. The minimum ground state energy or energy functional can be obtain through variational principle. After variational method process for the minimization of energy functional the Kohn-Sham equation can be written as

$$\left(-\frac{1}{2}\nabla^2 + V_s(\mathbf{r})\right)\psi_i = \varepsilon_i\psi_i \tag{2.13}$$

Here ψ is the wave function for single particle while ε is the corresponding state

energy and the last term in equation(2.13) is the effective potential $V_s(\mathbf{r})$, it can be written as

$$V_s(\mathbf{r}) = V_{ext}(\mathbf{r}) + \frac{\delta E_H(\rho)}{\delta\rho(\mathbf{r})} + \frac{\delta E_{xc}(\rho)}{\delta\rho(\mathbf{r})}$$

This effective potential can also be written as

$$V_s(\mathbf{r}) = V_{ext}(\mathbf{r}) + \frac{1}{2}\int \frac{\rho(\mathbf{r}')}{|\mathbf{r}-\mathbf{r}'|}d\mathbf{r}' + V_{xc}(\rho) \tag{2.14}$$

putting equation(2.14) back in equation(2.13) we get

$$\left(-\frac{1}{2}\nabla^2 + V_{ext}(\mathbf{r}) + \frac{1}{2}\int \frac{\rho(\mathbf{r}')}{|\mathbf{r}-\mathbf{r}'|}d\mathbf{r}' + V_{xc}(\rho) \right)\psi_i = \varepsilon_i\psi_i \tag{2.15}$$

This is the Kohn-Sham non interacting or equation for single orbital particle system it is very useful and effective in the condense matter physics. It is noticeable that it is the transformation of Schrodinger's many-body equation with full wave function Ψ to one particle orbital system with wave function ψ_i, to get the true density ρ. These are not the correct and true wave functions and energies. The only term if we can provide its true value we will get the true density of the system and that is the exchange correlation term. The exchange and correlation functional is the key term which contain all unknown information, providing the correct exchange correlation term or functional that will gives us the true density of the system. Though the Kohn-Sham many body equation is correct and can solve the many body problem theoretically but in reality more approximation has to be made. Some approximation can be made in the exchange correlation energy functional.

2.5 Exchange-correlation Functional

The exchange correlation functional is known as universal density approximation or universal density functional. Derivation of exchange-correlation energy is difficult

since it include many system. Fortunately this energy term can be approximated due to small energy comparatively with kinetic energy and Hartree energy. There are different methods for these approximations ,e.g., LDA [25], GGA [26] and Hybrid functionals [27, 28].

2.5.1 Local Density Approximation(LDA)

The approximation was proposed by Kohn-Sham with the DFT calculation in 1965. LDA functional is widely used in density functional theory calculations. This approximation is based on electron gas model known as homogeneous electron-gas (HEG) model, in which exchange part can be treated analytically. The exchange part is also energy which is a functional of density.

$$E_{xc}[\rho] = \int \rho(\mathbf{r})\varepsilon(\rho(\mathbf{r}))d\mathbf{r} \tag{2.16}$$

Where ε is the energy (exchange correlation energy)/electron in homogeneous gas with density(ρ). In an electron gas, infinite electrons travel in space of infinite volume, for neutralization of this gas an equal number of positive charges are distributed over this space [29]. Equation 2.5.1 is a general expression for exchange correlation energy functional, it can be made more effective by dividing it in to spin-up and spin-down. The approximation is known LDA(Local density Approximation) due to its dependence on local coordinates of that density.

$$E_{xc}[\rho] = \int \rho(\mathbf{r})\varepsilon[\rho_{\uparrow}(\mathbf{r}), \rho_{\downarrow}(\mathbf{r})]d\mathbf{r} \tag{2.17}$$

$\rho_{\uparrow}(\mathbf{r}), \rho_{\downarrow}(\mathbf{r})$ corresponds to spin polarized, spin-up and spin-down density, respectively. The exchange correlation energy is purely hypothetical guess or approximations, in reality neither positive charges nor electrons are uniformly distributed in molecules. It is further divided into exchange and correlation functionals The

parametrization was given by Perdew and Zunger which is implemented in QE package [30].

$$\varepsilon(\rho) = \varepsilon_x(\rho) + \varepsilon_c(\rho)$$

Where ε_x corresponds to exchange part and ε_c is the correlation functional term. LDA is good approximation for systems where density varies slowly. Calculations shows that LDA works well for many systems e.g in molecules, atoms and in solids. Generally LDA produce bonding which is stronger from actual system. It has some drawback also, like it underestimate the electronic band gap w.r.t experiments, and overestimation of bulk modulus due to underestimation of lattice parameters. Further approximations are required to improve the results of LDA calculations. In this thesis we used LDA.

2.6 Pseudopotential

Pseudopotential is another useful tool to reduce the computational cost of DFT calculations. As the name suggests that it is not the real potential or wave function, it is the potential which is used for the valance electrons instead of all electrons system. The behavior of the wave function near nucleus is almost the same for physical and chemical properties of a system. The valence electrons participate in bonding where we can say the core electrons are frozen. In other words the core electrons has the same properties for all systems. The wave function in equation 2.4 for density is expanded to a convenient basis set.The wave function with boundary conditions obey Bloch's theorem labeled with wave vector $\mathbf{k}$. The expansion of this set with boundary conditions is done using plane waves. The concept of plane wave was given by Herring in 1940 [31]. The main purpose of the pseudopotential is replacing

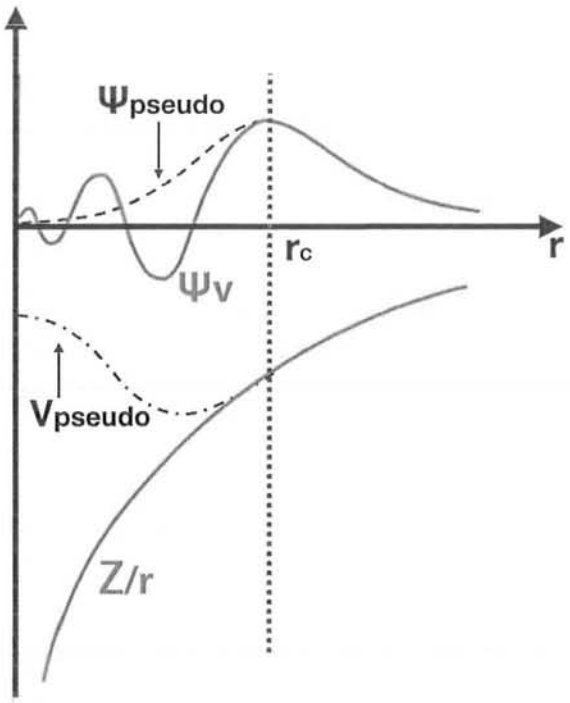

Figure 2.1: Representation for pseudo wave function and pseudopotential with real potential and wave function, where $\mathbf{r}_c$ is the cutoff radius.

strong Columb potential by an ionic effective potential for valance electrons. The real and pseudo wave function and potential are shown in Figure 2.1. Dash black line represents the pseudopotential and pseudo wave function, solid black line represents the radius and r_c is the cutoff radius on which the real and pseudo wave function and potentials agrees with the same results. Where the solid cyan lines represents the actual or real wave function and real potential. The pseudo wave function is node less where real wave function has many nodes before cutoff radius. Core region shows there is no radial nodes for the pseudo wave function. The pseudopotential is smoother from the all electron full potential in core region and is identical on and

beyond core radius. Smoother the wave function corresponds to less terms in the wave function, results in saving the computational time and cost. There are different types for pseudopotential e.g Normconserving pseudopotential and ultrasoft pseudopotential [32, 33].

2.6.1 Ultra-soft Pseudopotential

Making smoother and smoother the pseudo wave function as much as possible is the best technique to reduce the computational cost without losing the accuracy. Due to increase in the smoothness of pseudo wave function the range of the Fourier space decreases, which is important for the valence properties to certain accurate limit. In some cases it was noticed that the pseudopotential become, more expansive than actual all electron system, so a useful approximation was introduced by Vanderbilt. The Vanderbilt's approximation in the pseudopotential is known as Ultra Soft Pseudo Potential(USPP) [33]. Smoothness in the USPP is due to the modification of normconserving pseudopotential, which led to a smaller energy(cutoff energy) to expand the wavefunction in **k** space. As a result it saves the computational time and it also maintain the required accuracy. Figure 2.2 the solid line shows all electrons wave function, the doted line is the representation for normconserving pseudopotential and the dash line represents the ultra soft pseudopotential. It is clear from the fig. that ultra soft function is smoother and require fewer plane waves to reproduce. On the other hand normconserved pseudo wave function overlaps the actual all electron wave function.

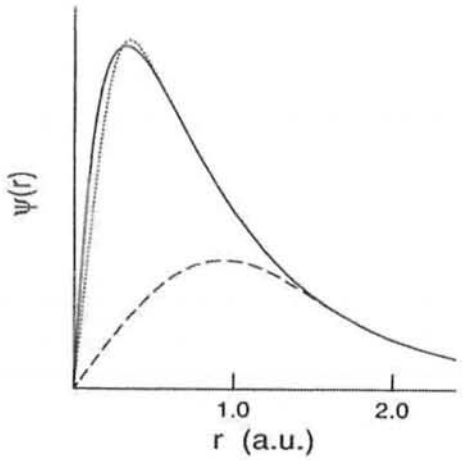

Figure 2.2: Comparison of Oxygen 2p radial wave function(solid line) with normconserved(doted line) and ultra soft pseudo(dash line) wave functions [33].

2.7 Quantum Espresso

We used quantum espresso for our computational calculations. Quantum espresso is a package used in first-principles calculations for electronic structure and material simulation [34], which is based on DFT, plane wave and pseudo potential. It is a popular and power full ab-initio tool in material simulation group worldwide. ESPRESSO stands for opEn Source Package for Research in Electronic Structure, Simulations and Optimization. It is available through out the world for researchers under GNU general public license [35]. This package includes many functions e.g, scf(self consistent field) calculations, pw.x(atomic relaxation), pp.x(post processing), projwfc.x(atomic projection), ph.x(phonon calculation) and wannier90.x(Wannier generation). The quantum espresso code solve the Kohn-Sham equations on iteration based, while the energy in a unit cell is optimized according to the positions of atoms in a unit cell.

2.8 BoltzTrap calculation

BoltzTrap is taken from Boltzmann transport theory [36–38], Boltzmann's equation is used to describe the behavior of fluid of electrons when they are not in thermodynamic equilibrium. Taking the possibility of approximate time relaxation, the expression for transport properties can be derived analytically e.g, electron thermal conductivity, Seebeck coefficient and electrical conductivity. The Fermi Dirac function which is a distribution function of a gas(electron) at equilibrium. If $\mathbf{k}$ is the state or wave vector and $\varepsilon_{\mathbf{k}}$ is the energy then average occupation number due to electrons is given by

$$f_{\mathbf{k}}^{0} = \frac{1}{e^{(\varepsilon_{\mathbf{k}}-\mu)/(k_B T)} + 1} \tag{2.18}$$

Where μ is chemical potential and k_B is Boltzmann constant. This function can vary with time as $f_{\mathbf{k}}(\mathbf{r}, t)$

$$\left(\frac{\partial f}{\partial t}\right) = \left(\frac{\partial f}{\partial t}\right)_{field} + \left(\frac{\partial f}{\partial t}\right)_{diff.} + \left(\frac{\partial f}{\partial t}\right)_{scatt.} \tag{2.19}$$

The first part of the equation on right side is acceleration of electrons by external field, the second term is diffusion due to temperature and the last term is scattering by phonons due to impurities or lattice defect. For steady state

$$\left(\frac{\partial f}{\partial t}\right)_{field} + \left(\frac{\partial f}{\partial t}\right)_{diff.} + \left(\frac{\partial f}{\partial t}\right)_{scatt.} = 0 \tag{2.20}$$

Using Liouville's theorem to solve Boltzmann's equation for $\mathbf{r}$ (position in space) at a specific time t.

$$f_{\mathbf{k}}(\mathbf{r}, t) = f_{\mathbf{k}}(\mathbf{r} - t\mathbf{v}_{\mathbf{k}}, 0)$$

$$\mathbf{v}_{\mathbf{k}} = \partial\varepsilon_{\mathbf{k}}/\partial\mathbf{k}$$

The second term in equation 2.20 becomes

$$\left(\frac{\partial f}{\partial t}\right)_{diff.} = \left(\frac{\partial f}{\partial T}\right).\left(\frac{\partial T}{\partial \mathbf{r}}\right).\left(\frac{\partial \mathbf{r}}{\partial t}\right) = -\left(\frac{\partial f}{\partial T}\right)\mathbf{v_k}.\nabla T \tag{2.21}$$

OR

$$\left(\frac{\partial f}{\partial t}\right)_{diff.} = \left(\frac{\partial f}{\partial \varepsilon_\mathbf{k}}\right)\left(\varepsilon_\mathbf{k} - \mu\right)\left(\frac{-\mathbf{v_k}\nabla T}{T}\right) \tag{2.22}$$

Similarly the field term after applying Liouville's theorem becomes

$$\left(\frac{\partial f}{\partial t}\right)_{field} = e\left(-\frac{\partial f}{\partial \varepsilon_\mathbf{k}}\right).\mathbf{v_k}E \tag{2.23}$$

The third term in equation 2.20 is complicated and energy dependent, applying the time relaxation approximation which is successful in many cases [39].

$$\left(\frac{\partial f}{\partial t}\right)_{scatt.} = \frac{f - f^0_\mathbf{k}}{\tau_\mathbf{k}} = -\frac{G_\mathbf{k}}{\tau_\mathbf{k}} \tag{2.24}$$

Where $G_\mathbf{k} = f - f^0_\mathbf{k}$ and $\tau_\mathbf{k}$ is carrier relaxation time. Putting the values of equations 2.22, 2.23 and 2.24 in 2.20 we get

$$G_\mathbf{k} = e\tau_\mathbf{k}\left(-\frac{\partial f}{\partial \varepsilon_\mathbf{k}}\right).\mathbf{v_k}E + \tau_\mathbf{k}\left(\frac{\partial f}{\partial \varepsilon_\mathbf{k}}\right)\left(\varepsilon_\mathbf{k} - \mu\right)\left(\frac{-\mathbf{v_k}\nabla T}{T}\right) \tag{2.25}$$

Relating this equation to the microscopic Ohm's law so we can get the transport properties of any material, as Ohm's law relates current density with temperature gradient and electric field

$$\mathbf{J} = \frac{1}{V}\sum_\mathbf{k} ef\mathbf{v_k} = \frac{1}{V}\sum_\mathbf{k} eG_\mathbf{k}.\mathbf{v_k} \tag{2.26}$$

As current density is zero at equilibrium

$$\textstyle\sum_\mathbf{k} ef^0_\mathbf{k}\mathbf{v_k} = 0$$

V represents volume in real space, putting equation 2.25 in equation 2.26

$$\mathbf{J} = \frac{1}{V}\sum_\mathbf{k} e\mathbf{v_k}\left[e\tau_\mathbf{k}\left(-\frac{\partial f}{\partial \varepsilon_\mathbf{k}}\right).\mathbf{v_k}E + \tau_\mathbf{k}\left(\frac{\partial f}{\partial \varepsilon_\mathbf{k}}\right)\left(\varepsilon_\mathbf{k} - \mu\right)\left(\frac{-\mathbf{v_k}\nabla T}{T}\right)\right] \tag{2.27}$$

$$\mathbf{J} = \frac{1}{V}\sum_{\mathbf{k}} e^2 \tau_{\mathbf{k}} \mathbf{v}_{\mathbf{k}} \mathbf{v}_{\mathbf{k}} \left(-\frac{\partial f}{\partial \varepsilon_{\mathbf{k}}} \right) \cdot \left[E + \frac{1}{eT} \frac{\sum_{\mathbf{k}} \tau_{\mathbf{k}} \left(-\frac{\partial f}{\partial \varepsilon_{\mathbf{k}}} \right) (\varepsilon_{\mathbf{k}} - \mu) \mathbf{v}_{\mathbf{k}} \mathbf{v}_{\mathbf{k}} (-\nabla T)}{\sum_{\mathbf{k}} \tau_{\mathbf{k}} \left(-\frac{\partial f}{\partial \varepsilon_{\mathbf{k}}} \right) \mathbf{v}_{\mathbf{k}} \mathbf{v}_{\mathbf{k}}} \right] \tag{2.28}$$

Ohm's law (macroscopic Ohm's law)

$$\mathbf{J} = \overleftrightarrow{\sigma} \left(E + \overleftrightarrow{S} (-\nabla T) \right) \tag{2.29}$$

Where $\overleftrightarrow{S}$ is Seebeck coefficient also known thermopower and $\overleftrightarrow{\sigma}$ is electrical conductivity tensors. We can get the values of $\overleftrightarrow{S}$ and $\overleftrightarrow{\sigma}$ by comparing equation 2.28 and 2.29.

$$\overleftrightarrow{\sigma} = \frac{e^2}{V} \sum_{\mathbf{k}} \tau_{\mathbf{k}} \left(-\frac{\partial f}{\partial \varepsilon_{\mathbf{k}}} \right) \mathbf{v}_{\mathbf{k}} \mathbf{v}_{\mathbf{k}} \tag{2.30}$$

$$\overleftrightarrow{S} = A (\overleftrightarrow{\sigma})^{-1} \tag{2.31}$$

Where $[A = \frac{e}{TV} \sum_{\mathbf{k}} \tau_{\mathbf{k}} \left(-\frac{\partial f}{\partial \varepsilon_{\mathbf{k}}} \right) (\varepsilon_{\mathbf{k}} - \mu) \mathbf{v}_{\mathbf{k}} \mathbf{v}_{\mathbf{k}}]$. Similarly we can find the expression for electron thermal conductivity by following the procedure for heat current, for electron.

$$\overleftrightarrow{\kappa}_{elec.} = \frac{1}{VT^2} \sum_{\mathbf{k}} \tau_{\mathbf{k}} \left(-\frac{\partial f}{\partial \varepsilon_{\mathbf{k}}} \right) (\varepsilon_{\mathbf{k}} - \mu)^2 \mathbf{v}_{\mathbf{k}} \mathbf{v}_{\mathbf{k}} \tag{2.32}$$

From these expressions for electrical conductivity, thermopower and electron thermal conductivity we can see that electrical conductivity and thermopower are inversely related, Weidemann law tells that electron thermal conductivity and electrical conductivity are directly related. Increasing thermopower results in decreasing electrical conductivity, while increasing electrical conductivity increases electron thermal conductivity. This shows a complicated relationship for figure of merit, So obtaining highly efficient thermoelectric material is not a simple task.

2.9 Computational details

We studied the electronic and thermoelectric properties of $LiNbO_2$ using first-principles calculations which is based on density functional theory (DFT). We used the plane-wave pseudopotential method [40] with a plane-wave cut-off of 60 Ry and Ultra-soft pseudopotential as implemented in the Quantum-ESPRESSO code. To get the ground-state charge density and electronic wave function, we used local-density approximation (LDA) for the exchange and correlation potential. Boltzmann transport theory (BoltzTrap) was used for the calculation of thermoelectric properties of $LiNbO_2$ as a function of carrier concentration (both p-type and n-type) and as a function of temperature. For the computation of thermoelectric parameters and electronic calculations we used k-meshes ranging from $2\times2\times2$, $6\times6\times6$, $20\times20\times20$ and $40\times40\times40$ for different systems.

2.10 Motivation

Different thermoelectric (TE) materials are discovered in the past, but most of them are very expansive or toxic. That's why oxides TE materials are the center of attention. Oxide materials with layered structure are considered to be the best candidate for TE performance. $LiNbO_2$ has layered structure and could be considered a suitable material for thermoelectric applications due to its remarkable properties.
In nonstoichiometric $LiNbO_2$ the octahedral site are flexible with respect to Li vacancies. The increase in electrical conductivity and decrease in thermal conductivity could be expected due to intrinsic defects in $LiNbO_2$. Hence, it is expected that intrinsic defects (Li or O vacancies) can improve the TE properties of $LiNbO_2$. The main goal of the present work to optimized the TE performance of $LiNbO_2$ by con-

sidering both electron and hole carrier concentrations. We also study the electronic and TE properties of Ta and Ni doped $LiNbO_2$.

Chapter 3

Results and Discussions

3.1 Electronic Structure of $LiNbO_2$

The electronic structure of $LiNbO_2$ and its transport thermoelectric properties(TE) were calculated using Q.Espresso code. To calculate the thermoelectric properties of $LiNbO_2$ different arrangement were used for a good thermoelectric material, like doping, creating vacancy in $LiNbO_2$ etc. We can find the properties of a material through Hamiltonian by providing some basic information regarding structure, chemistry and atomic position of that material. While the information about structure of any element or material or compound are determined through its lattice constant. Lattice constant for exchange and correlation functional and plane wave basis set can be calculated using different approximation like LDA and GGA.

Using Quantum Espresso code, we optimized the lattice parameters of $LiNbO_2$ using LDA approximation. As $LiNbO_2$ has hexagonal crystal structure [15], we have optimized lattice constant (a) and (c/a), where $8 \times 8 \times 4$ k-point mesh were used for optimizing both parameters lattice constant (a) and (c/a). The calculated lattice

parameters (a) and (c/a) with previous work are shown in table3.1. The calcu-

Table 3.1: Comparison of calculated lattice parameters with previous work.

Parameters	This work	Previous work
a (Å)	2.882	2.908[a] 2.912[b] 2.912[c] 2.90[d]
c/a	3.614	3.59 [a] 3.592[b] 3.589[c] 3.60[d]

[a] Reference [15] [b] Reference [16]

[c] Reference [19], [d] Reference [20]

lated values a and c/a nearly matches with experimental work [20], e.g, calculated a= 2.882 and c/a = 3.614, whereas experimental values are a =2.90 and c/a = 3.60 [20], there is a small difference of 0.7% in a and 0.4% in c/a. Similarly these calculated values are also in good agreement with the other values from the previous work, with a small difference. This calculated data does not matches exactly with previous work, because LDA always underestimates the values.

The optimized lattice parameters "a" and "c/a" are shown in Fig. 3.1(a), Fig. 3.1(b), respectively, lattice constant in atomic unit on x-axis and minimum to maximum energy in Rydberg on the y-axis can be seen. We used these optimized lattice parameters a and c/a in further calculations, like band structure, density of state, partial density of state etc. The bonding orbitals and anti-bonding orbitals interact and they form energy bands. The bonding orbitals interact and they form valance band while the anti-bonding orbitals interact to form conduction band. The gap between these two bands is known as the band gap or forbidden gap. This is the

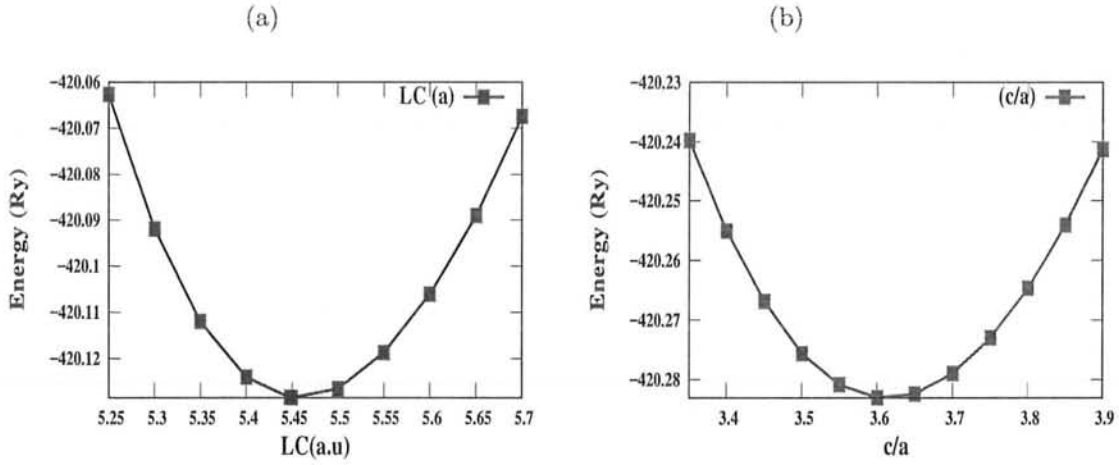

Figure 3.1: Optimized lattice parameters (a) lattice constan a in atomic unit on x-axis and energy in Rydberg on y-axis, (b) c/a on x-axis and energy in Rydberg on y-axis.

difference of energies between valance and conduction band energies. The band structure and density of state shows the nature of the material like whether it is conductor, semiconductor or insulator. It also tells about the conduction and valence band, while partial density of state shows the contribution of each and every atom to these valance and conduction bands. The direct and indirect band gap are categorized on the basis that if the valance band maximum and conduction band minimum lies on the same symmetry point, if not then call indirect band gap. The calculated band structure for $LiNbO_2$ is shown in Fig. 3.2. The band structure is calculated using the optimized lattice parameters, and a direct band gap was observed as was predicted by Novikov *et al.*, [17]. Our calculated direct band gap is about 1.67 eV, whereas there is some disagreement about the band gap of $LiNbO_2$ in literature, e.g, a band gap of 1.5 eV was reported by Novikov *et al.* [17], while 2 eV band gap was also reported from Geselbracht *et al.* [18]. We can see the valance band maximum and the conduction band minimum on the same point, which is

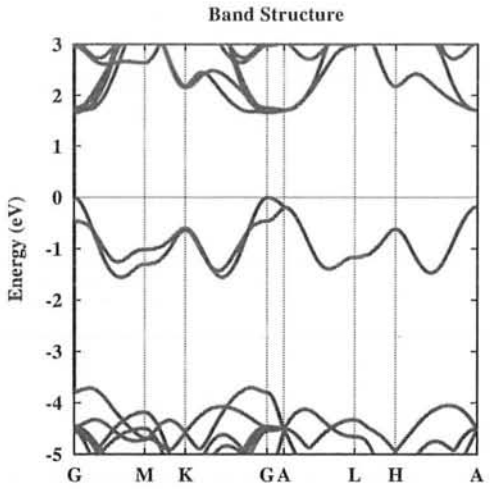

Figure 3.2: Calculated band structure of $LiNbO_2$, the horizontal line represents the valence band maximum.

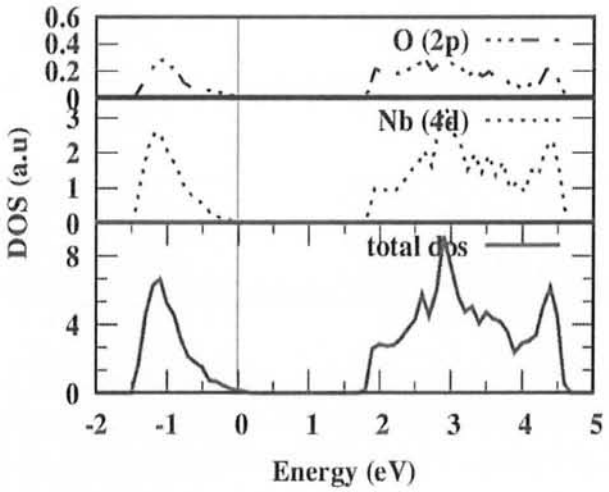

Figure 3.3: Calculated DOS and PDOS of $LiNbO_2$, total DOS(solid line), Nb-d(dots line) and O-2p(combine dash and dots line), the vertical line corresponds to Fermi level.

represented by "G ".

Density of state (DOS) is the number of different states which electron are allowed to occupy at a specific energy level. DOS and partial or projected density of state were calculated and plotted in Fig.3.3. This figure consists of three mini figures, which represents the total density and partial density of states, red (solid line) represents the total density of state while the blue (dots line) and black (combine dash,dots line) represents the partial or projected density of state. As the maximum contribution to total DOS of $LiNbO_2$ is from Nb-4d (dots blue line) orbital and then oxygen 2p (combine dash,dots black line) orbital, as shown in Fig.3.3. The maximum contribution to valence band was 15% from O-2p and the rest was from Nb-4d and no contribution from Li atom calculated which is also predicted in article Ref. [?]. The Fermi level is at 0 eV, we can calculate the band gap from here also, the gap between valance and conduction band which is about 1.67eV. In agreement with the calculated value of band structure. So $LiNbO_2$ is a direct band gap semiconductor with a band gap of 1.67eV in these calculation.

The electronic charge density is visualized using XCrySDen. It is a tool which is easily available and can be used for visualizing molecular and crystalline structure without any extra software in Linux [41]. The calculated charge density along (100) plane for $LiNbO_2$ pure system is shown in Fig.3.4. The charge density tells us qualitatively about the bonding nature of the material, e.g, how much charge is localized on which atom, and how much is transfered to which atom? In our case comparatively the valance charge density is maximum on oxygen, less on niobium atom while on lithium the charge density is very small. It shows covalent bonding nature between Nb and O atom, while ionic bonding for $LiNbO_2$. The electronegativity in periodic table is Li $<$ Nb $<$ O, mostly charges are localized on oxygen

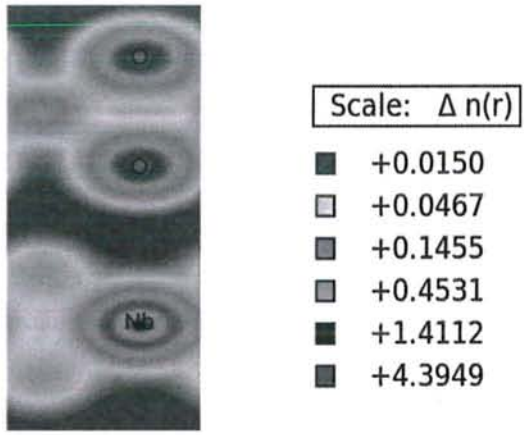

Figure 3.4: Electronic valance charge density of $LiNbO_2$

atom.

3.2 T.E parameters as a function of chemical potential

Thermoelectric properties of $LiNbO_2$ were calculated using different systems like different chemical potentials with different temperatures, hole doping, electron doping carrier concentrations with different temperatures, creating vacancy in super-cell of $liNbO_2$, like lithium vacancy and oxygen vacancy with different temperatures. The thermoelectric parameters were calculated with different chemical potential at a fixed temperatures as well as with different temperatures at fixed chemical potentials, these all combinations are discussed one by one. The behavior of thermoelectric parameters are calculated and observed for fixed temperature with different chemical potentials, the calculated parameters are shown in Fig.3.5. Where Fig.3.5[(a)-(e)] corresponds to Seebeck coefficient, electrical conductivity (σ), thermal conductivity (κ), power factor (PF) and figure of merit (ZT), respectively. These calculations were carried out for three different fixed temperatures 300K, 500K and 800K rep-

resented by blue, green and red color lines, respectively. In these calculations the vertical line shows the Fermi energy level. The chemical potential is positive for n-type doping and negative for p-type doping. The maximum absolute value for Seebeck coefficient is 2835.37 μ V/K at 0.0645 Ry (Fig.3.5(a)). Similarly the value of Seebeck coefficient is 237.55 μ V/K at $\mu = 0$ Ry. When S > 0 at $\mu = 0$, it implies that it is a p-type semiconductor. Using BoltzTrap we can find electrical conductivity with scattering time as (σ/τ), using this calculated value and comparing it with the experimental value of electrical conductivity, i.e., 49 cm^{-1} Ω^{-1} [42], and following the procedure used of P.Ong *et al.*, [43], we got the value of scattering time ($\tau' = 4.0 \times 10^{-15}$sec). Then we further used this value of scattering time in our calculations for electrical conductivity and thermal conductivity.

Electrical conductivity and thermal conductivity has its maximum values 2169 (k S/m) and 39.55 $Wm^{-1}K^{-1}$ at 0.2146 Ry and 0.229 Ry, respectively having temperature 300K. The value of thermopower is decreasing with temperature, while electron thermal conductivity is increasing, which is according to Weidemann's law. While the electrical conductivity is slightly affected by temperature as discussed in section in 1.6.The band gap between valance band maximum and conduction band minimum is 0.123 Ry or 1.67 eV. Peaks occurs in the conduction region for different temperatures in Seebeck coefficient, electrical conductivity and thermal conductivity. DOS in Fig.3.3 shows the same trend, the peaks of DOS and peaks of Fig.3.5(c) are almost at the same energy 0.223 Ry or 3 eV. As the positive chemical potential refers to n-type carriers, so the highest occupied state by electron is from the contribution of Nb-d, and O-p orbitals. Fig.3.5(d) and Fig.3.5(e) are power factor and figure of merit. The edges of conduction band minimum and valance band maximum in PF shows that PF is better for n-type $LiNbO_2$. In ZT we use electron thermal

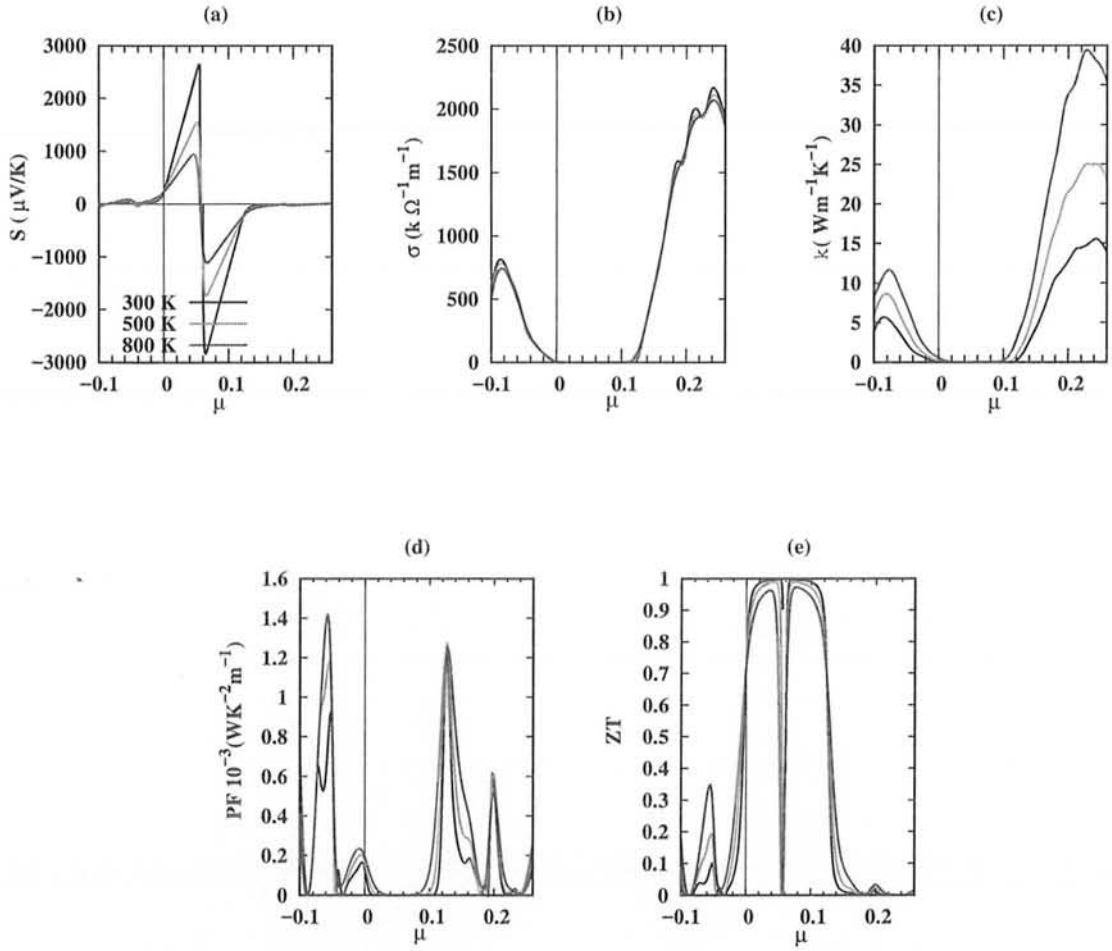

Figure 3.5: The thermoelectric parameters of $LiNbO_2$ as a function of chemical potential(Ry) at 300, 500 and 800K temperature. (a) Seebeck coefficient, (b) electrical conductivity, (c) thermal conductivity, (d) power factor and (e) figure of merit.

conductivity only and the lattice thermal conductivity is not added with it. The figure of merit is approaching to unity at 0.0687 Ry at 300K temperature.

3.2.1 T.E parameters as a function of carrier concentrations

In this section the behavior of thermoelectric parameters are calculated at constant temperature with carrier concentrations. Carrier concentration varied from 10^{18} to 10^{21} /cm^3. Thermoelectric parameters were calculated for both cases e.g electron doped and hole doped carrier concentrations as shown in Fig.3.6 and Fig.3.7, respectively. Where the temperature was kept constant and the number of carrier concentrations were varied. These calculations were carried out for different temperature 300, 400, 500, 600, 700, and 800K, which are shown in Fig.3.6(a) and Fig. 3.7(a). Similarly these colors represents the same temperature in (b), (c), (d) and (e) in both Fig.3.6 and Fig.3.7. From Fig.3.6 these thermoelectric parameters are calculated for electron doped carrier concentrations. Fig.3.6(a) corresponds to thermopower, the Seebeck coefficient is increasing with temperature and its value is decreasing with carrier concentrations which is in accordance with Pisarenko's relation discussed in section 1.5.

The absolute maximum value of thermopower is 850 μV/K at temperature 800K and number of carrier concentration is 1.26×10^{18}/cm^3. Fig.3.6(b) is the calculated value for electrical conductivity. The electrical conductivity is directly proportional to carrier concentration and inversely linked to temperature, discussed already in section 1.6. Calculating electrical conductivity at constant temperature, we used the experimental value of electrical conductivity 49cm^{-1} Ω^{-1} from Ref. [42] at 300K, which is compared with our DFT value σ/τ, we got the value of scattering time, while the number of carrier concentration n is found by using the experimental

value of Seebeck coefficient (180 μV/K) at 300K [42]. For different temperatures σ is plotted as

$$(\sigma/\tau) * (C/(n^{\frac{1}{3}} * T)) \tag{3.1}$$

Where $C = \tau' * T * n^{1/3}$ and τ' is the experimental value of scattering time. For figure of merit the experimental lattice thermal conductivity, e.g, (κ_l = 2.47, 1.90 and 1.60 W/m^{-1}K^{-1} for 400, 600 and 800K respectively) from Ref. [42] is added with electron thermal conductivity and total thermal conductivity is simplified as $[(\kappa/\tau) * (C/(n^{\frac{1}{3}} * T)) + \kappa_l]$ where σ/τ and κ/τ are the DFT calculated values.

The maximum value of electrical conductivity is 6 (kS/m) at 300K and at 10^{21} electron carrier concentration/cm^3, and is going on decreasing with increasing temperature. While the electron thermal conductivity is minimum at low temperature and is increasing with increasing temperature as indicated in Wiedemann's law. Fig.3.6(d) is power factor which has its maximum value at low temperature, 300K and 3.99×10^{20} carrier/cm^3. While Fig.3.6(e) represents figure of merit, which has its maximum value at high temperature and high number of carrier concentrations. The maximum value of ZT is 0.245 at 800K and 9.97×10^{20} carrier/cm^3 and is going on decreasing with decreasing temperature. As discussed earlier that we have included the value of lattice thermal conductivity for different temperature in figure of merit.

Similarly Fig.3.7[(a)-(e)] corresponds to thermopower, electrical conductivity, thermal conductivity, power factor and figure of merit, respectively. These are the plots for thermoelectric parameters which are calculated for hole doped carrier concentrations/cm^3. Following the same procedure for hole doped, as followed in electron doped concentrations. We can see the results of different parameters for different fixed temperature, e.g, 300, 400, 500, 600, 700 and 800K.

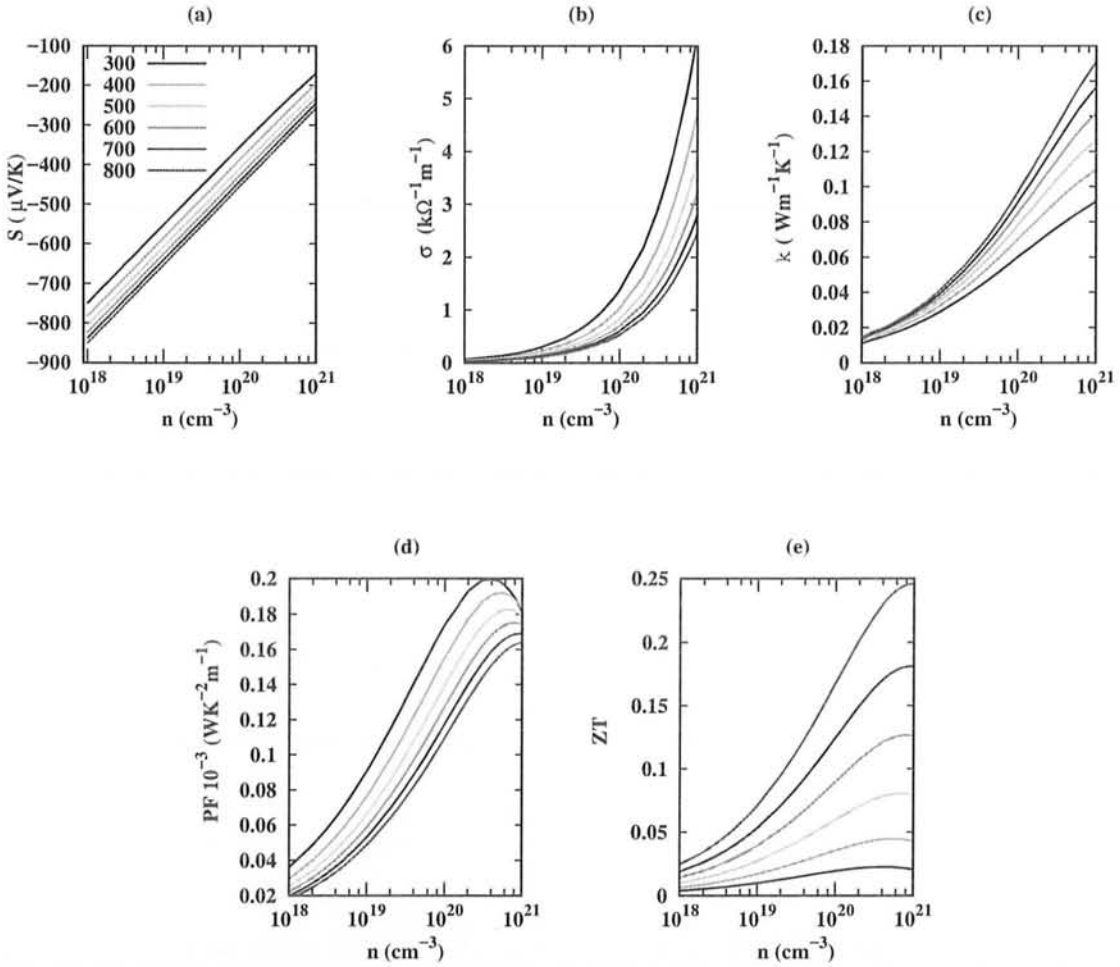

Figure 3.6: Electron doped thermoelectric parameters of $LiNbO_2$ at diffenent temperatures. (a), (b), (c), (d) and (e) represents thermopower, electrical conductivity, electron thermal conductivity, power factor and figure of merit, respectively.

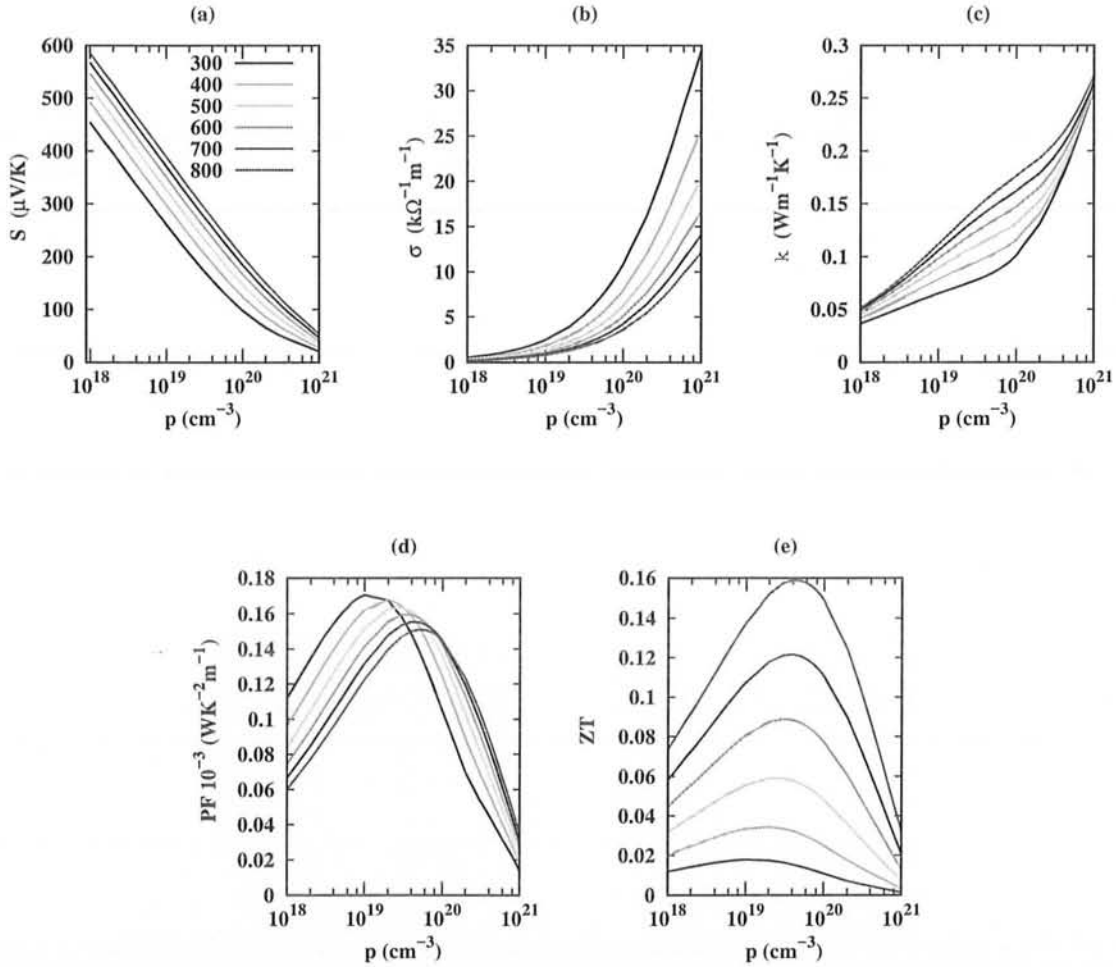

Figure 3.7: Hole doped thermoelectric parameters of $LiNbO_2$ at diffenent temperatures. (a), (b), (c), (d) and (e) represents thermopower, electrical conductivity, electron thermal conductivity, power factor and figure of merit respectively.

Fig.3.7(a) thermopower has its maximum value at 800K temperature with 1.02×10^{18} concentration/cm^3, and decreasing with increasing concentration, at room temperature its maximum value is 455 (μV/K).

Electrical conductivity Fig.3.7(b) has its maximum value at low temperature 300K and at higher concentration. Electrical conductivity decreases at higher temperatures, even at higher carrier concentrations (10^{21}/cm^3) its value at 800K temperature is 12.3 (k S/m). Electron thermal conductivity inversely behaves with temperature as compared with electrical conductivity. Power factor (Fig. 3.7(d)) has its maximum value at low temperature and the number of carrier concentrations are 10^{19}/cm^3. Anyhow the peaks are shifting towards higher concentrations with higher temperatures. The maximum value of power factor at 300K is 0.17×10^{-3}WK^{-2}m^{-1} at 10^{19}/cm^3, and slightly decreasing at higher temperature. Similarly the figure of merit (Fig. 3.7(e)), has its maximum value 0.158 at 800K, with 4.8×10^{19} carrier concentrations/cm^3, and decreasing with higher temperatures.

Comparing both electron doped and hole doped $LiNbO_2$, we can see that electron doped thermoelectric properties are better as compared with hole doped properties. Maximum value of thermopower at 300K for electron doped is 750 (μV/K), while its value for hole doped concentrations is 450 (μV/K) at the same temperature. Similarly the most important parameter in thermoelectric properties is ZT, which is also larger for electron doped as compared to hole doped. Using the technique of S. Hao *et al.*, [44] procedure we found that effective mass of electron in this case is greater than the effective mass of hole, which is more dominant in Seebeck (Pisarenko's [10] relation), and hence in figure of merit.

3.3 T.E Parameters as a function of Temperature

In this section the thermoelectric parameters for $LiNbO_2$ at different fixed or selected electron doped and hole doped carrier concentration were calculated as a function of temperature. The calculated thermoelectric parameters at electron carrier concentrations (10^{18}-10^{21}) as a function of temperature (300K-800K) are shown in Fig. 3.8. Following the same procedure as followed in section 1.5, for electron thermal conductivity, electrical conductivity, power factor and figure of merit. First these values were calculated with scattering time, then we find the value of scattering time from experimental value of electrical conductivity and multiplied it with these terms. The absolute value of thermopower is increasing with increasing temperature, similarly thermal conductivity, power factor and ZT are also increasing with increasing temperature.

Comparing these calculated parameters to our previous section for electron doped concentrations, thermopower in section 3.2.1 has its maximum value for 800K, Fig. 3.6(a) at $10^{18}/cm^3$ carrier concentration. In this section, Fig. 3.8(a) also shows its maximum value for electron doped 10^{18} (bold line) concentration at 800K. While the slight difference in electrical conductivity and thermal conductivity is due to the scattering time, because we multiplied different values of scattering time for different temperature in previous calculations. Here we used one fixed value of scattering time (4.066×10^{-15} sec) for all temperatures. Thats why the ZT has larger maximum value (0.4) in this section instead of (0.245) section 3.2.1 Fig. 3.6(e) at higher concentrations and 800K.

The thermoelectric parameters for $LiNbO_2$ at different fixed hole doped carrier concentrations as a function of temperature are shown in Fig. 3.9. The Fig. 3.9[(a)-

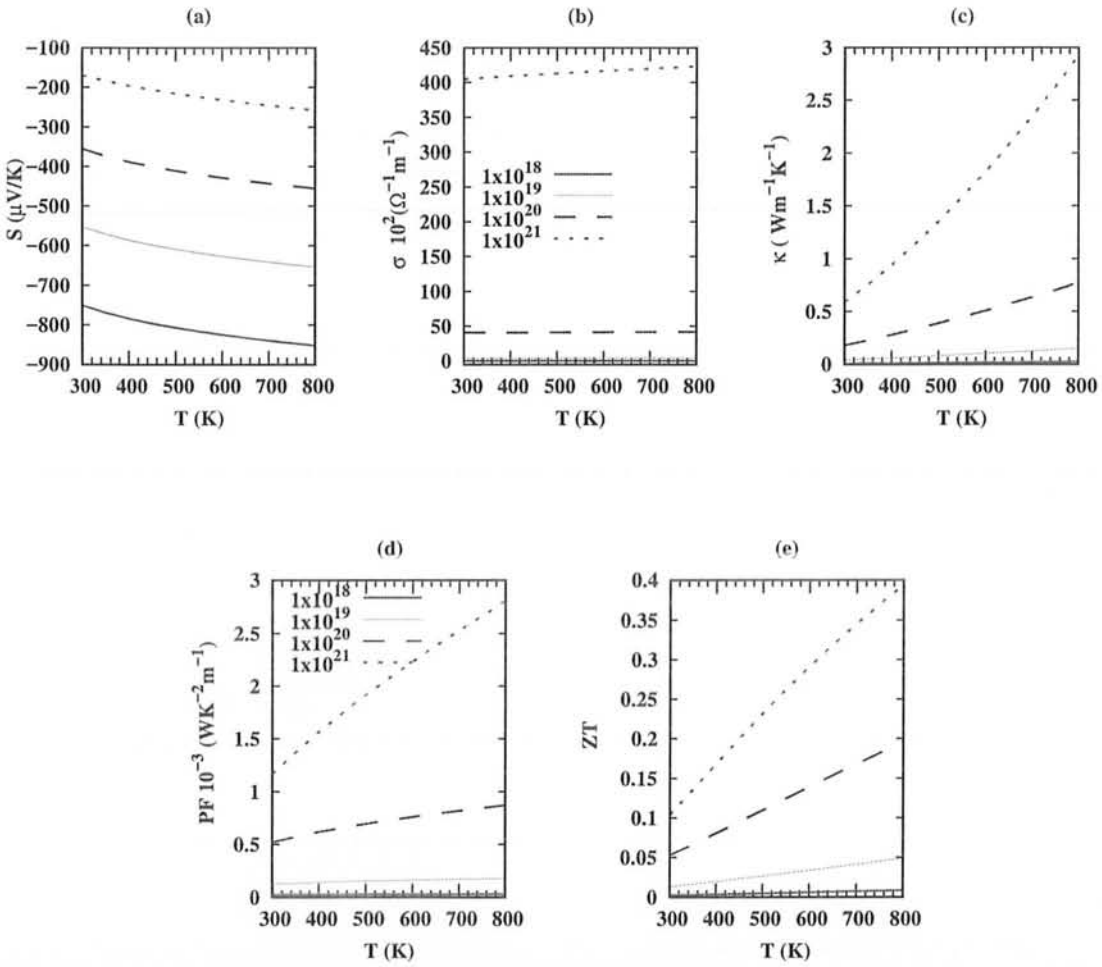

Figure 3.8: Electrons doped thermoelectric parameters of $LiNbO_2$ at fixed carrier concentrations 1×10^{18}(bold line), 1×10^{19}(solid line), 1×10^{20}(dash line), and $1\times10^{21}/cm^3$(dots line) as a function of temperatures.

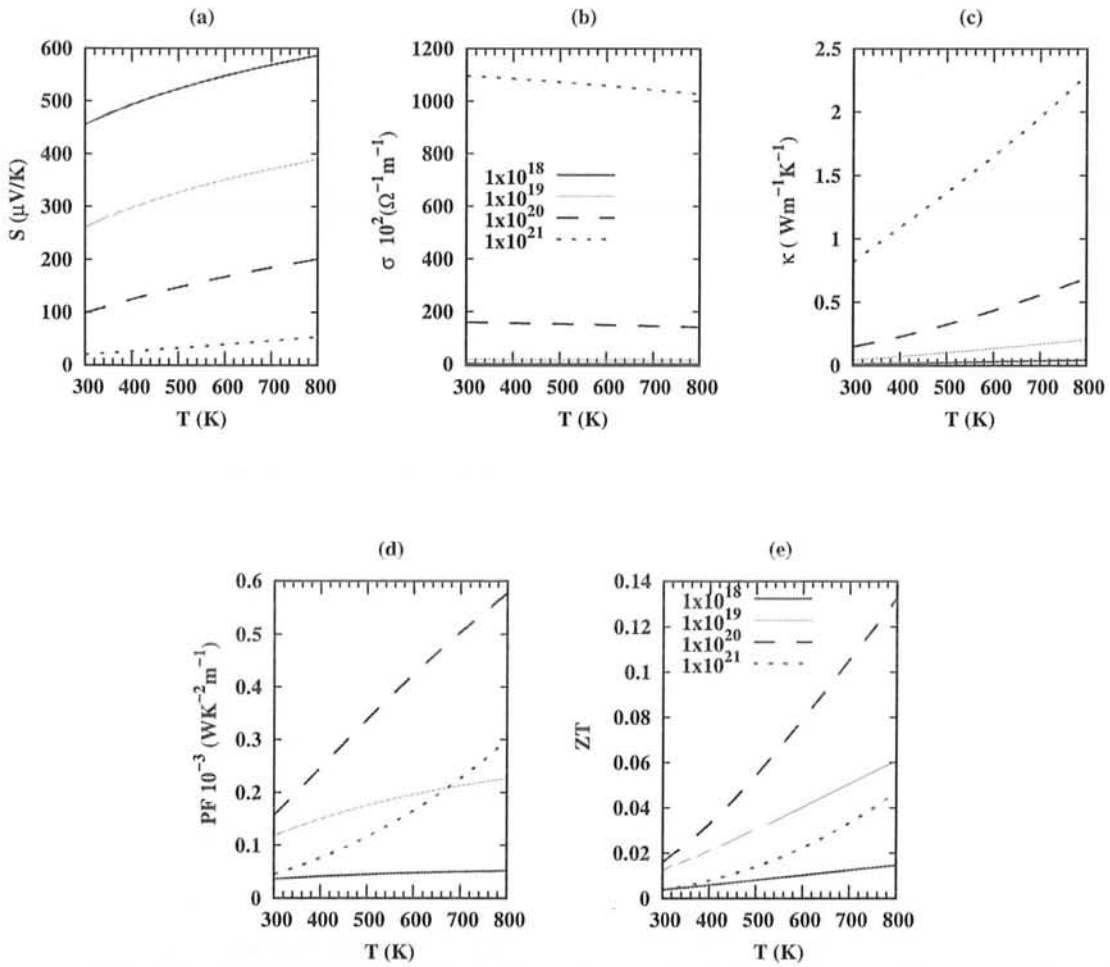

Figure 3.9: Holes doped thermoelectric parameters of $LiNbO_2$ at fixed carrier concentenration 1×10^{18}(bold line), 1×10^{19}(solid line), 1×10^{20}(dash line), and $1\times10^{21}/cm^3$(dots line) as a function of temperatures.

(e)] corresponds to Seebeck coefficient, electrical conductivity, thermal conductivity, power factor and figure of merit, respectively. The fixed number of carrier concentrations are represented with different lines, e.g, bold line, solid line, dash line and dots line corresponds to 1×10^{18}, 1×10^{19}, 1×10^{20} and $1\times10^{21}/cm^3$, respectively. If we compare these calculated parameters with our previous calculations in section (3.2.1), we can see these thermoelectric parameters are in good agreement. If we compare the Seebeck coefficient of Fig. 3.7(a) and Fig. 3.9(a), it verifies values of each other completely. Maximum value of thermopower at room temperature 300K is 450 (μV/K) in both cases, e.g, hole doped concentration as a function of temperature and as a function of carrier concentration/cm^3. While the minimum value of Seebeck coefficient in both cases at 800K is 586.6 (μV/K).

Similarly for other thermoelectric parameters the results are almost similar with each other for both cases, and the small difference is due to the scattering time. As there is no need of scattering time in Seebeck coefficient so it matches in both sections. In this section we used one fixed value of scattering time, but in that previous calculations the value of scattering time varies with temperature.

3.4 $LiNbO_2$ Supercell

A crystal structure is the combination of many small unit cells, if the crystal structure is made from the same unit cell with larger volume, those cell are called supercell. $LiNbO_2$ supercell has 64 atoms with (16) Li, (16) Nb and (32)oxygen atoms. Figure 3.10 is the repetition of $LiNbO_2$ 8 atoms small unit cell in x,y and z-axis, e.g, $LiNbO_2$ (2×2×2) supercell. As the lattice parameters are increased by making the supercell of $LiNbO_2$, k-points used for scf and nscf calculations were used 2×2×2

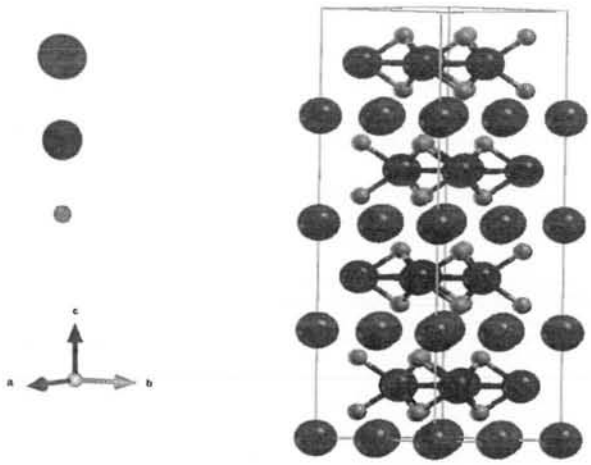

Figure 3.10: $LiNbO_2$ Supercell composed of 64 atoms including 16 Li, 16 Nb and 32 oxygen atoms.

and 6×6×6 respectively. For simplicity giving name to this supercell "System 01". The calculated band structure and DOS for System 01 are shown in Fig. 3.11 and Fig. 3.12, respectively. The band gap in both band structure and DOS is equal to the results obtained for pure $LiNbO_2$ (8 atoms) unit cell. Similar results were observed for thermoelectric parameters also. As it is understood that supercell is the repetition of the small unit cell so its properties will be similar to that small unit cell, thats why we did not included the calculated thermoelectric parameters for System 01 here. The reason for making this supercell is that we created vacancies and doped other different atoms in this System 01 with a small ratio, so we can observe the behavior of thermoelectric parameters or T.E efficiency of $LiNbO_2$ by adding or creating small amount of impurities in this material. For that purpose we did calculations for creating Li vacancy (removing 1/16 of Li) atom, oxygen vacancy (removing 1/32 of oxygen) atom from $LiNbO_2$ supercell. Similarly 1/16 of Li atom was replaced by Ta atom, doping Ta by replacing 1/16 of Nb atom and doping Ni

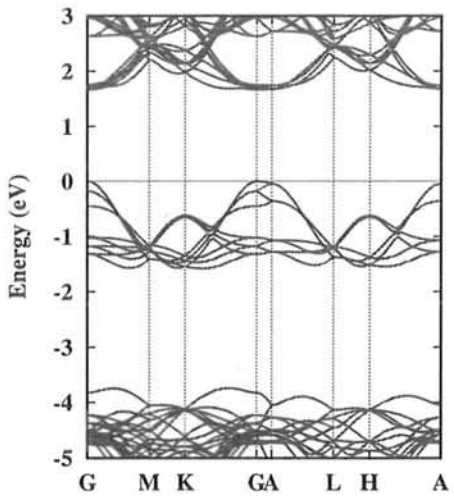

Figure 3.11: The calculated electronic band Structure of System 01. The horizontal line represents the valence band maximum.

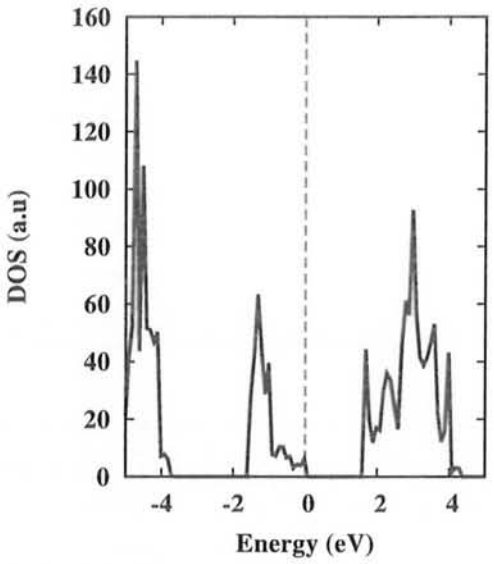

Figure 3.12: The calculated total density of state for System 01, the vertical dash line represents the Fermi level.

with with same ratio instead of Li atom. Naming them System 02 (Li vacancy), System 03(oxygen vacancy), System 04(Ta at Li site), System 05(Ta at Nb site) and System 06(Ni at Li site).

The thermoelectric parameters, e.g, thermopower, electrical conductivity, electron thermal conductivity, power factor and figure of merit were calculated for all these systems as a function of temperature one by one.

3.5 Formation Energy

The formation energy is an important factor for any defected material in DFT, it tells us about a material whether it is stable or not. The formation energy can be calculated for vacancy created material as well for defect or impurity added to a material. Vacancy formation energy is very important quantity which tell us about the concentration of vacancies in a material. This quantity can be defined as the energy required to remove the atom from the host material and place it into a reservoir of the same specimen. The formation energy is related with defects that can be calculated in a situation when an atom is removed or added to a material, which changes the properties of the original material.

The formation energy indicates whether the impurity added to a material or a vacancy created in a material is possible or not. Lower formation energy tells us that the impurity can be added to a material or lower formation energy of a material due to vacancy is possible. On the other hand the higher formation energy indicates the material is unstable. The material of our interest is $LiNbO_2$ doping and creating vacancy in this material. The formation energy can be calculated as [45]

$$E_f = E_{def} - E_{pure} + n\mu_A - n\mu_B \tag{3.2}$$

$$E_f = E_{def} - E_{pure} + n\mu_A \tag{3.3}$$

E_f is the formation energy, E_{def} is the total energy of the material when it is defected by adding impurity or creating vacancy, n is the number of defected atoms, μ_A is the chemical potential for atom (A=Li,Nb,O) which is replaced or removed and μ_B is the chemical potential of (B=Ta,Ni), B is the dopant atom (which is added to the system). μ_A, μ_B are calculated as the total atom energy and Equation 3.2 is the formation energy for a material in which an atom A is replaced by another atom B, while equation 3.3 is the formation energy for a material in which vacancy is created.

We calculated formation energy for different systems, e.g, Li vacancy, O vacancy system, Ta doped at Li site, Ta doped at Nb site and Ni doped at Li site, table 3.2. Among these systems all values are positive, only Sys 05 has a negative sign so it

Table 3.2: Formation energy of System 02-06(Li vacancy, oxygen vacancy, Ta at Li site, Ta at Nb site and Ni at Li site.

System	E_{def}	E_{pure}	μ_A	μ_B	E_f(Ry)	E_f(eV)
Sys 02	-3347.475	-3362.2870	-14.643		0.169	2.298
Sys 03-01	-3328.431	-3362.2870	-33.229		0.627	8.527
Sys 04	-3500.349	-3362.2870	-14.643	-153.189	0.484	6.577
Sys 05	-3387.577	-3362.287	-127.907	-153.189	-0.008	-0.109
Sys 06	-3447.432	-3362.287	-14.643	-100.166	0.378	5.140

indicates that Ta at Nb site is most stable among these combination. Ta and Nb both belongs to the same group in the periodic table and their oxidation state is also the same so it may be the reason for the stable state of Ta at Nb site $LiNbO_2$

supercell, while Sys 03-01(oxygen vacancy) is most unstable as it has the larger positive value among other. The formation energy of Sys 02(Li vacancy) is smaller compared with the positive values of the other systems so it is stable to occur in our list after Ta at Nb site. So the most favorable and stable System is Ta at Nb site $LiNbO_2$, in our calculation using DFT.

3.6 T.E Properties due to vacancy systems

In this section we have calculated the thermoelectric properties of Li and oxygen vacancy systems, as a function of temperature. $Li_{1-x}NbO_2$ where (x=0.0625) Li vacancy system and $LiNbO_{2-y}$ (y = 0.0313) is oxygen vacancy system. The reason for doing these calculations is that, we already calculated the thermoelectric properties of $LiNbO_2$ with large amount of hole and electron carrier concentrations, here we want to find thermoelectric properties for small number of hole and electron concentrations.

3.6.1 Li Vacancy Supercell

The calculated electronic band structure and DOS of System 02 are shown in Fig. 3.13 and 3.14, respectively, where the vertical dash line in total DOS represents the Fermi level. We can see the Fermi level is shifted towards the valance band in both figures which was expected for Li vacancy, as creating Li vacancy produce hole in valance band so there are more hole as compared to electron in Li vacancy $LiNbO_2$ as shown in Fig. 3.13. Band structure and density of states shows some extra states on valance band which is due to the creation of hole in System 01. The band gap is reduce to 1.176 eV due to this defect, which can be seen from DOS and band

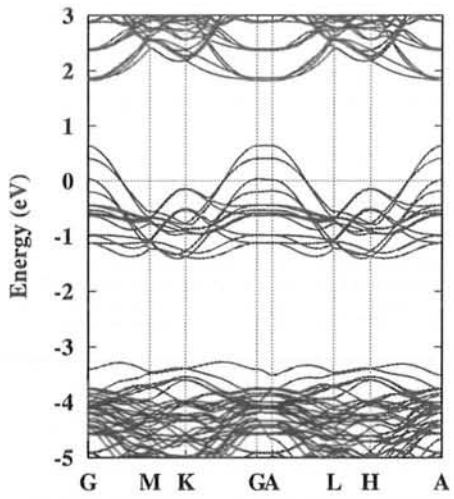

Figure 3.13: Band Structure of System 02, the horizontal line represents the valance band maximum.

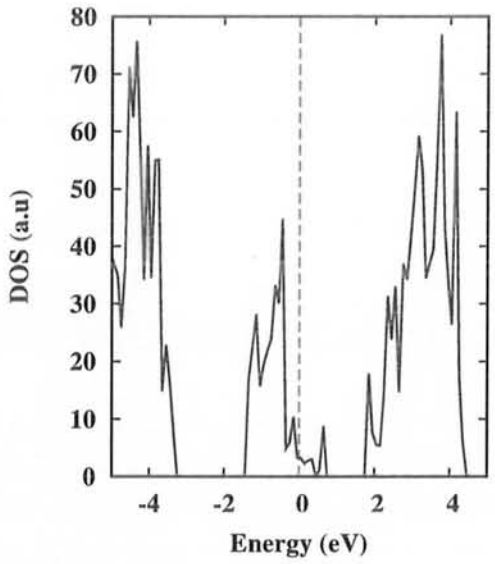

Figure 3.14: The calculated density of state of System 02, the vertical dash line represents the Fermi level.

structure. The structure of $LiNbO_2$ distorts due to Li vacancy, Li vacancy cause increase in lattice parameter c. The repulsive forces between O and its opposite sheets increases due to Li vacancy, which results decrease in the band gap.

The thermoelectric properties for System 02 are calculated as a function of temperature (Fig. 3.15). The temperature is varied from 300 to 800K for all thermoelectric parameters, while the chemical potential was kept constant 0.996 Ry, this is the chemical potential at Fermi level. From Fig. 3.15(a) the minimum and maximum values of Seebeck coefficient are 18 and 52 μV/K at 300 and 800K. The Seebeck coefficient at 300K or room temperature is 18 μV/K and is increased with increasing temperature. The sign of thermopower is positive for all temperature ranges from 300 to 800K indicates that the majority carrier are holes. Fig. 3.15(b) shows that the electrical conductivity has its minimum and maximum values of 128 and 131 k(S/m) at 300 and 800K, the scattering time used here is 4×10^{-15} s.

A small change in thermal conductivity is also observed ranges from 0.99 to 1.8 (W/mK) for temperature range 300 to 800K. Fig. 3.15[(d) and (e)] corresponds to power factor and figure of merit. Power factor has its maximum value 0.35×10^{-3} W/mK^2. The experimental value of lattice thermal is added in ZT with thermal conductivity i.e $\kappa = \kappa_e + \kappa_l$. So we can see the maximum and minimum values of ZT are 0.0038 and 0.0199 for 300 and 800K respectively. The results calculated for ZT here in System 02 are approximately in good agreement with experimental work [42]. They did their experiment for $Li_{1-x}NbO_2$ at different x, x=0, 0.05, 1.0, where we did our calculations for x=0.0625, so in comparison with x=0.05 the results for ZT in our calculations are almost equal to their experimental results.

Comparing TE coefficients of this p-type Li vacancy with the TE coefficients of hole doped $LiNbO_2$. We can see that the Seebeck coefficient of hole doped $LiNbO_2$ at

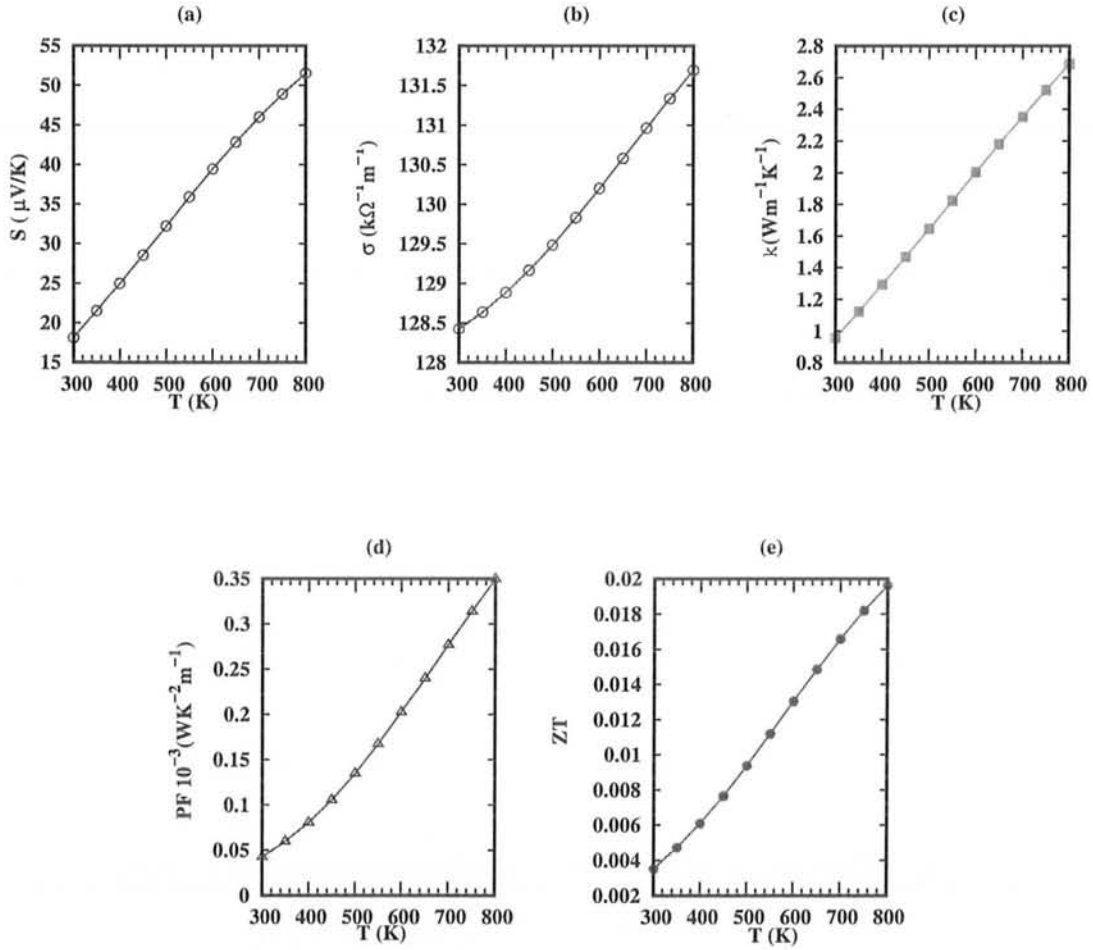

Figure 3.15: Thermoelectric parameters of System 02 as a function of temperature. (a) Seebeck coefficient, (b) electrical conductivity, (c) thermal conductivity, (d) power factor and (e) figure of merit.

(1×10^{21} carrier concentration/cm^3) almost matches with Li vacancy system. The minimum value of hole doped system is 20.7 μV/K, whereas 18 μV/K for Li vacancy at 300K. While the other TE coefficients e.g, thermal conductivity is 2.7 W/mK for Li vacancy and 2.3 W/mK for hole doped system at 800K. Similarly power factor and figure of merit are 0.3 W/mK^2 and 0.043 for hole doped system and 0.35 W/mK^2 and 0.02 for Li vacancy at 800K. Different possibilities were searched for further improvement in the thermoelectric efficiency of $LiNbO_2$.

3.6.2 Oxygen vacancy Systems

In this section we have done the TE calculations for oxygen vacancy systems. Oxygen vacancy is further divided in three systems, System 03-01, System 03-02 and System 03-03. These all systems are same except, the lattice constant (a) is decreased and increased 2% in System 03-02 and System 03-03, respectively from System 03-01. The band structure, total DOS and T.E properties were calculated for all these three systems.

The calculated band structure for these three systems are shown in Fig. 3.16. Fig. 3.16(a) corresponds to System 03-01, Fig. 3.16(b) is band structure for System 03-02 and Fig. 3.16(c) is the band structure for System 03-03. The extra states in the conduction band can be seen in all three systems, indicating that oxygen vacancy cause majority electron carrier. So System 02 was a p-type material and System 03(including 01, 02 and 03) is an n-type material. The band gap is increased for System 03-02 in which we decreases the lattice constant (a) 2%, while the band gap decreases for System 03-03. The gap energy is inversely proportional to the square of lattice constant [46]. Decreasing lattice constant causing the decrease in the inter atomic distances. The valance electron become more bounded by decreasing the

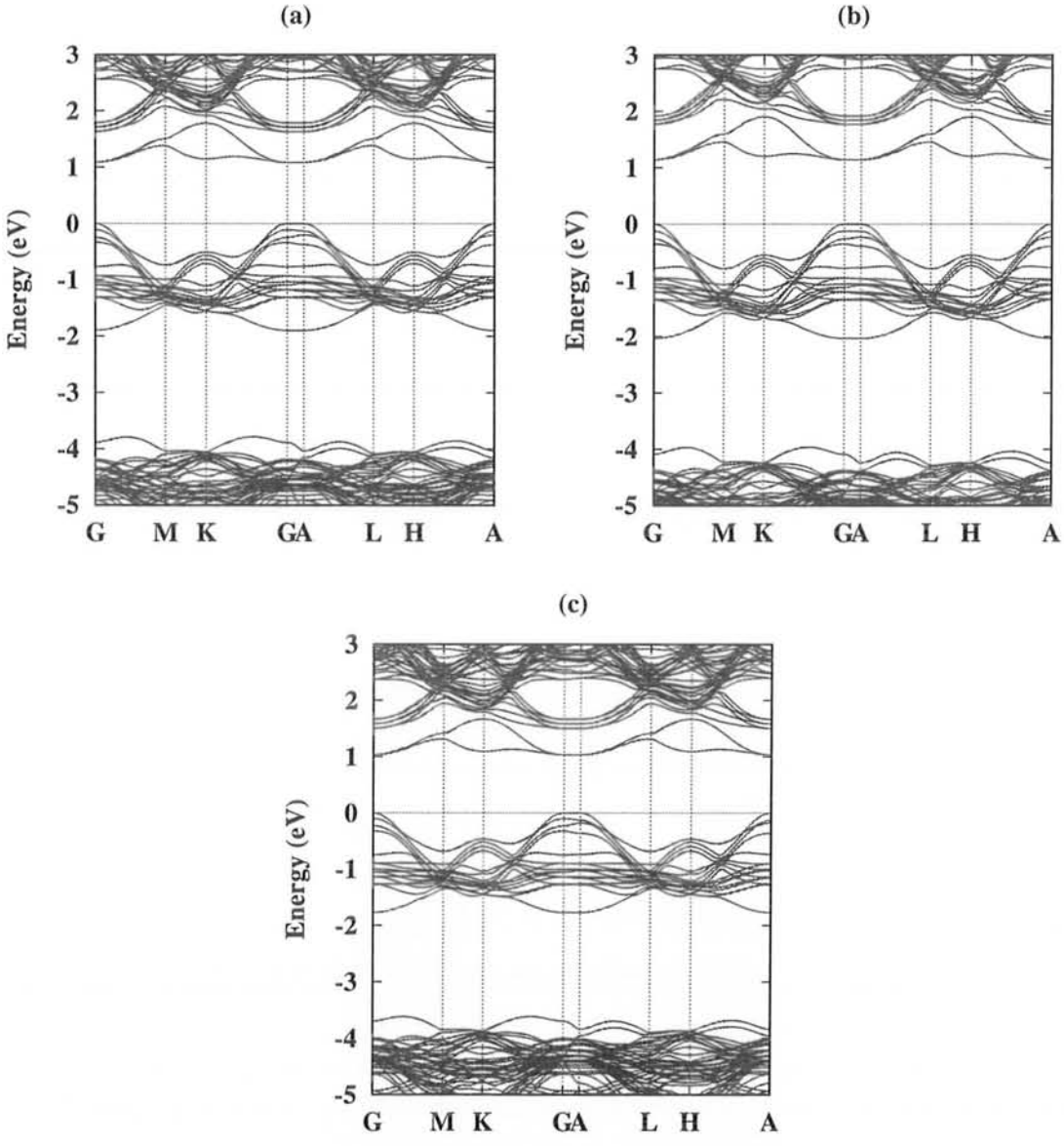

Figure 3.16: Calculated electronic band structure of System 03-01 (a), System 03-02 (b) and System 03-03 (c). The horizontal line corresponds the valence band maximum.

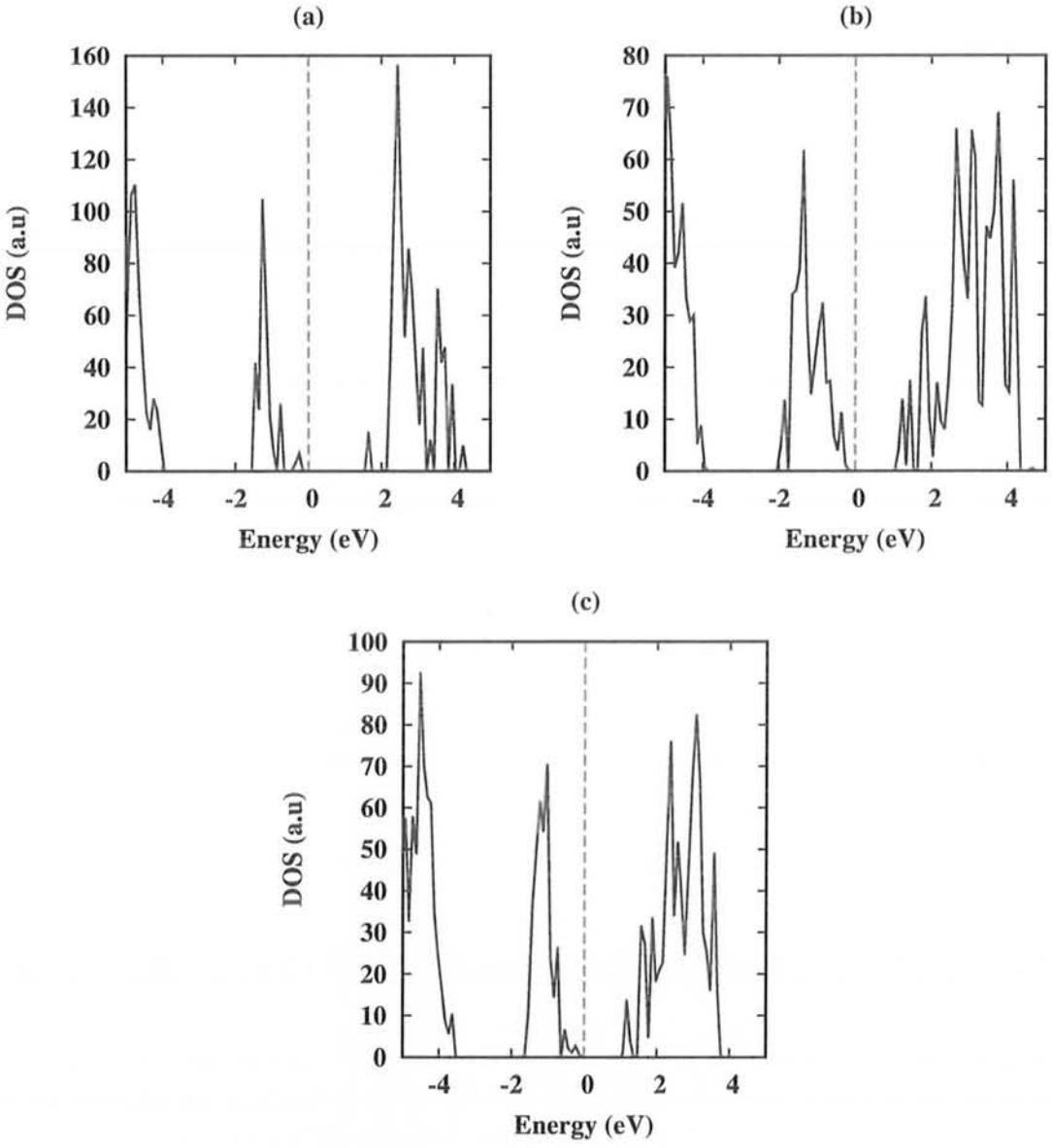

Figure 3.17: Calculated total DOS of system 03, (a), (b) and (c) are System 03-01, System 03-02, and System 03-03. The dash line represents the Fermi level.

lattice constant so more energy is required for these electron to become free in the upper band(conduction band). The results calculated for total density of states in Fig. 3.17 agrees with these changes in band gap. Fig. 3.17(a), Fig. 3.17(b) and Fig. 3.17(c) corresponds to System 03-01, System 03-02 and System 03-03 respectively. The dashed line represents the Fermi level in Fig. 3.17[(a)-(c)].

A band gap of 1.67 eV is calculated for System 01, here the band gap for System 03-01 is equal to 1.087 eV, 1.142 eV for System 03-02 and 1.032 eV for System 03-03. The thermoelectric properties of these systems are calculated and are shown in Fig. 3.18. The solid line, dash line and dots line in Fig. 3.18 corresponds to System 03-01, System 03-02 and System 03-03, respectively. In Fig. 3.18 the thermopower is calculated with chemical potential at conduction band, because oxygen vacancy in $LiNbO_2$ behaves as an n-type impurity. So the sign of thermopower is negative for these systems as shown in Fig. 3.18(a) for each system. The absolute value of S first slightly decreases and then increases to its maximum at 800K. For System 03-01 the minimum value of S is 211 μV/K at 600K.

The comparison of these thermoelectric parameters are shown in table 3.3. The

Table 3.3: Comparing T.E parameters of oxygen vacancy systems(oxygen vacancy and 2% decrease and increase in lattice parameter a of oxygen vacancy) at 800K.

System	S(μV/K)	σ(kS/m)	κ_e(Wm^{-1}K^{-1})	PF 10^{-3}(Wm^{-1}K^{-2})	ZT
Sys 03-01	-336.5	17.4	0.60	1.97	0.182
Sys 03-02	-300	18.57	0.64	1.68	0.152
Sys 03-03	-352.3	16.75	0.56	2.07	0.194

absolute value of Seebeck coefficient and other thermoelectric parameters are taken

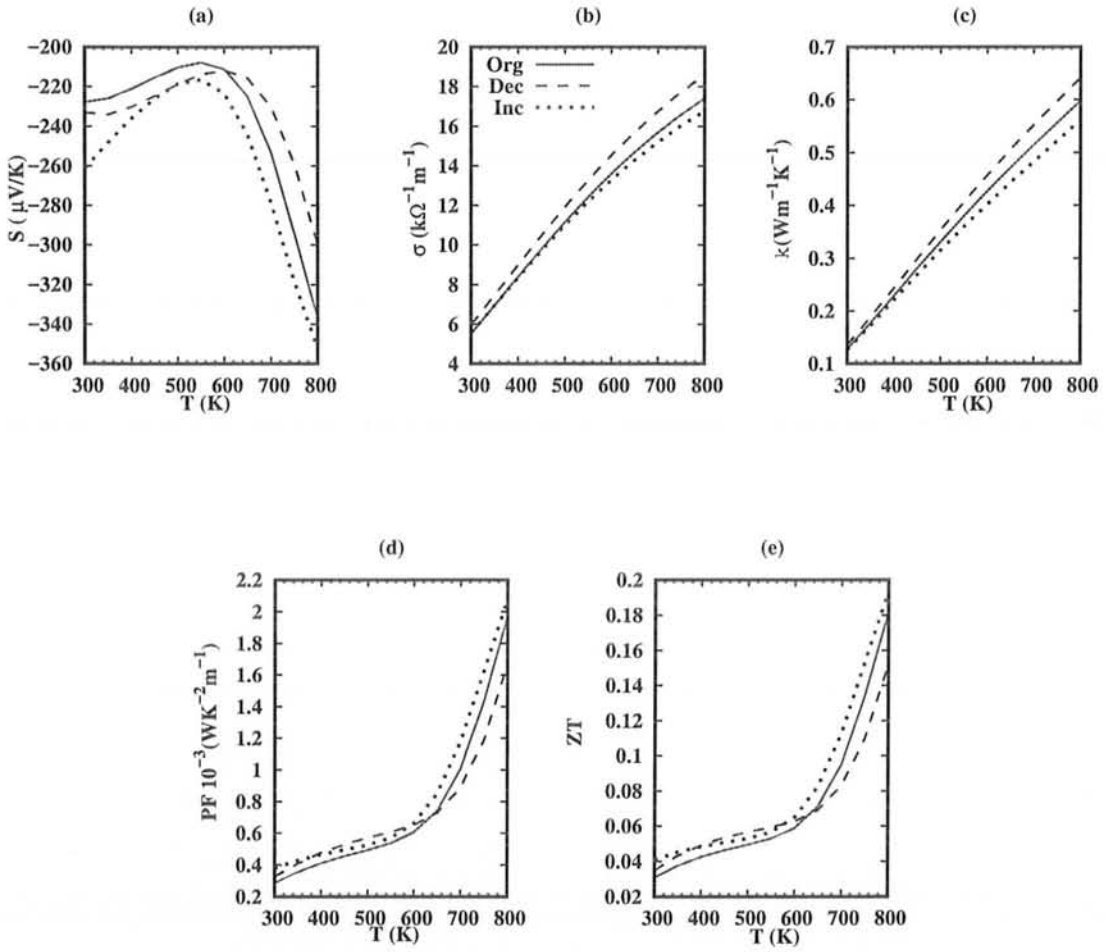

Figure 3.18: Thermoelectric parameters of System 03-01 (solid line, denoted as Org), System 03-02 (dash line, denoted as Dec) and System 03-03 (dots line, denoted as Inc), as a function of temperature. (a) Seebeck coefficient, (b) electrical conductivity, (c) thermal conductivity, (d) power factor and (e) figure of merit.

here at higher temperature, i.e., 800K. According to these results the Seebeck coefficient is larger in System 03-03. Electrical conductivity is higher in System 03-02, similarly electron thermal conductivity is also maximum in System 03-02. Power factor is larger in System 03-03 because of S, which is more dominant in power factor. The value of figure of merit(ZT) is 0.182, 0.152 and 0.194 for System 03-01, System 03-02 and System 03-03 respectively. The value of ZT is higher in System 03-03, thus the efficiency of this system is better than other two systems. Here strain can improve the TE properties of $LiNbO_2$.

3.7 T.E Properties of Doped Systems

We have calculated the density of states, band structure and thermoelectric properties for doped systems in this section. Doped systems means, adding some impurities or amount of other atoms to Sys 01, e.g, doping Ta atom at Li site, Ta at Nb site and doping Ni at Li site. Ta at Li site $Li_{1-x}Ta_xNbO_2$ (x=0.0625) is System 04, Ta atom at Nb site $LiNb_{1-x}Ta_xO_2$ (x=0.0625) is System 05 and Ni at Li site $Li_{1-x}Ni_xNbO_2$ (x=0.0625) is System 06 in our list. Fig. 3.19(a) is the band structure of System 04 in which the Fermi level is shifted towards the conduction band. While Fig. 3.19(b) is the band structure of System 05 which looks similar to the band structure of System 01, it has a direct band gap at gamma point with an energy gap of 1.64 eV, where Fig. 3.19(c) corresponds to System 06 having some extra states on valance band and decrease in the band gap also. It shows an indirect band gap, where the valance band maximum is on point L and the conduction band minimum lies between gamma and point K. The band gap in this system is reduced to 1.43 eV.

Similarly the total density of state for these three systems are calculated and

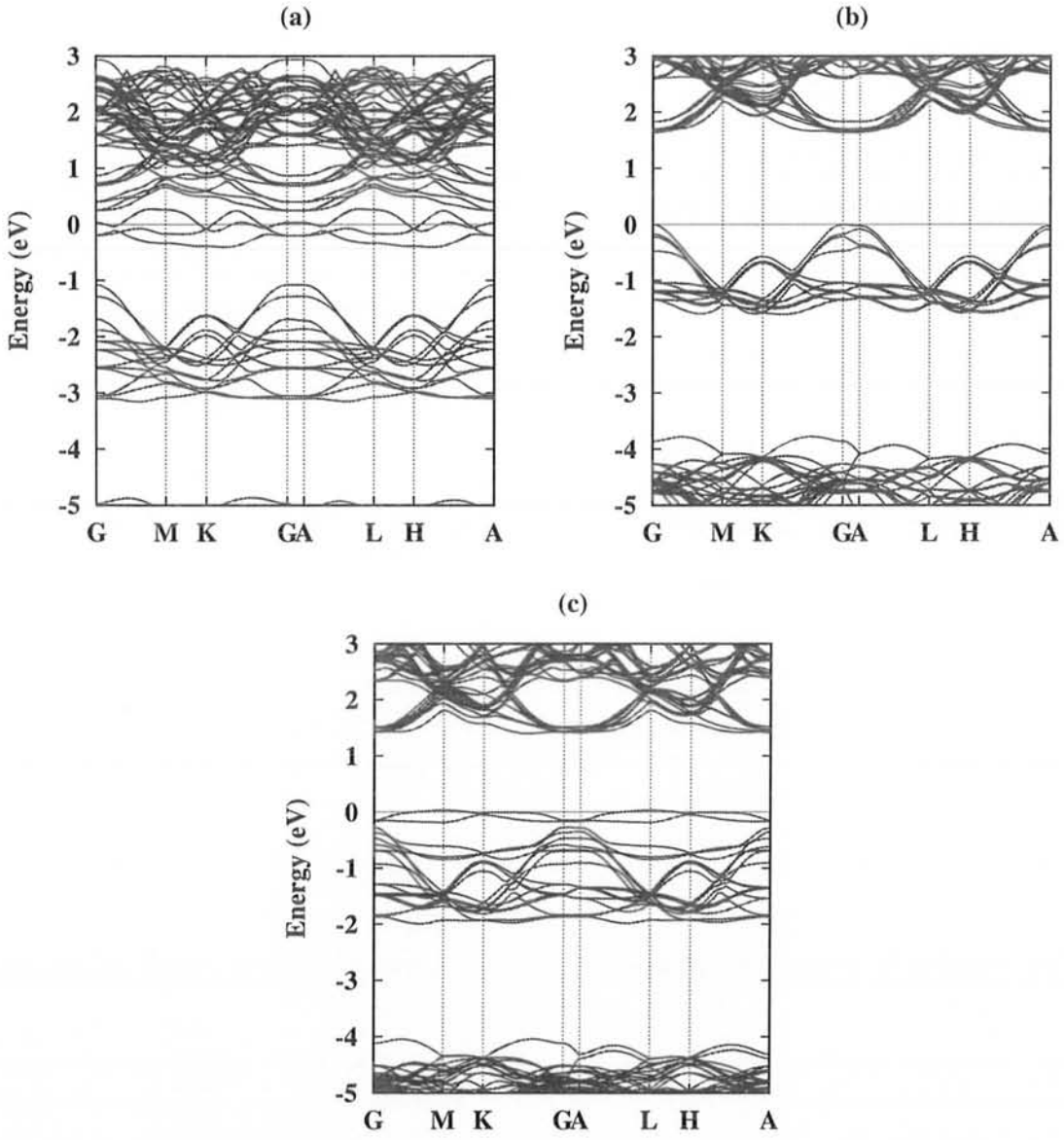

Figure 3.19: Calculated electronic band structure of System 04 (a), System 05 (b) and System 06 (c). The horizontal line represents the valence band maximum.

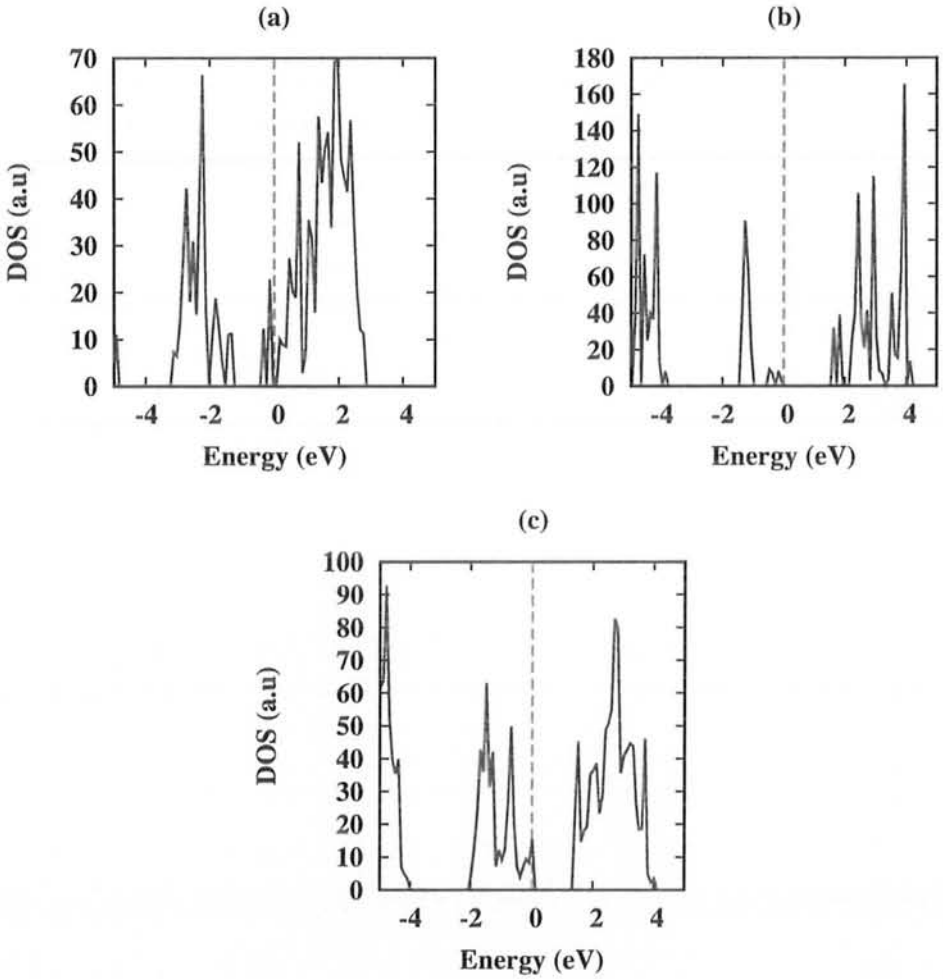

Figure 3.20: The total calculated DOS of doped systems, System 04 (a), System 05 (b) and System 06 (c). The dash line corresponds to Fermi level.

shown in Fig. 3.20. Fig. 3.20(a), Fig. 3.20(b) and Fig. 3.20(c) corresponds to the total DOS of System 04, System 05 and System 06, respectively. The vertical dash line in these figure shows the Fermi level, the chemical potential near to Fermi level is used in these calculation. DOS of System 04 shows that it has the Fermi level which is shifted towards the conduction band as shown in band structure calculation. Fig. 3.20(c) is the total DOS of System 06 which shows the slight shift of Fermi level towards valance band.

Thermoelectric properties of these systems are calculated and shown in Fig. 3.21, Fig. 3.22 and Fig. 3.23, which correspond to T.E properties of System 04, System 05 and System 06, respectively. These calculations are done at constant chemical potential as a function of temperature. Doping Ta at Li site, Li has only one valence electron while Ta has three valence electrons, so doping Ta at Li site results majority electron carriers. That's why thermopower or Seebeck coefficient in Fig. 3.21(a) is negative. The minimum absolute value of Seebeck coefficient is 56 μV/K at 300K temperature. The value of Seebeck coefficient is increasing with temperature is reached to a maximum absolute value of 100 μV/K at 800K temperature. While the electrical conductivity decreases with temperature as shown in Fig. 3.21(b), the maximum value of electrical conductivity is 57 (kS/m) at 300K temperature, at higher temperature its value reduces to 54 (kS/m) at 800K. The electron thermal conductivity, power factor and ZT increases with increasing temperature as shown in Fig. 3.21(c), Fig. 3.21(d) and Fig. 3.21(e), respectively.

The minimum value of thermal conductivity is 0.4 ($Wm^{-1}K^{-1}$) at 300K temperature and reaches to its maximum value 0.85 ($Wm^{-1}K^{-1}$) at 800K. Power factor is increasing with temperature, due to Seebeck coefficient which is dominant as compared to electrical conductivity. The minimum value of PF is 0.17 $10^{-3}(Wm^{-1}K^{-2})$, at 300K

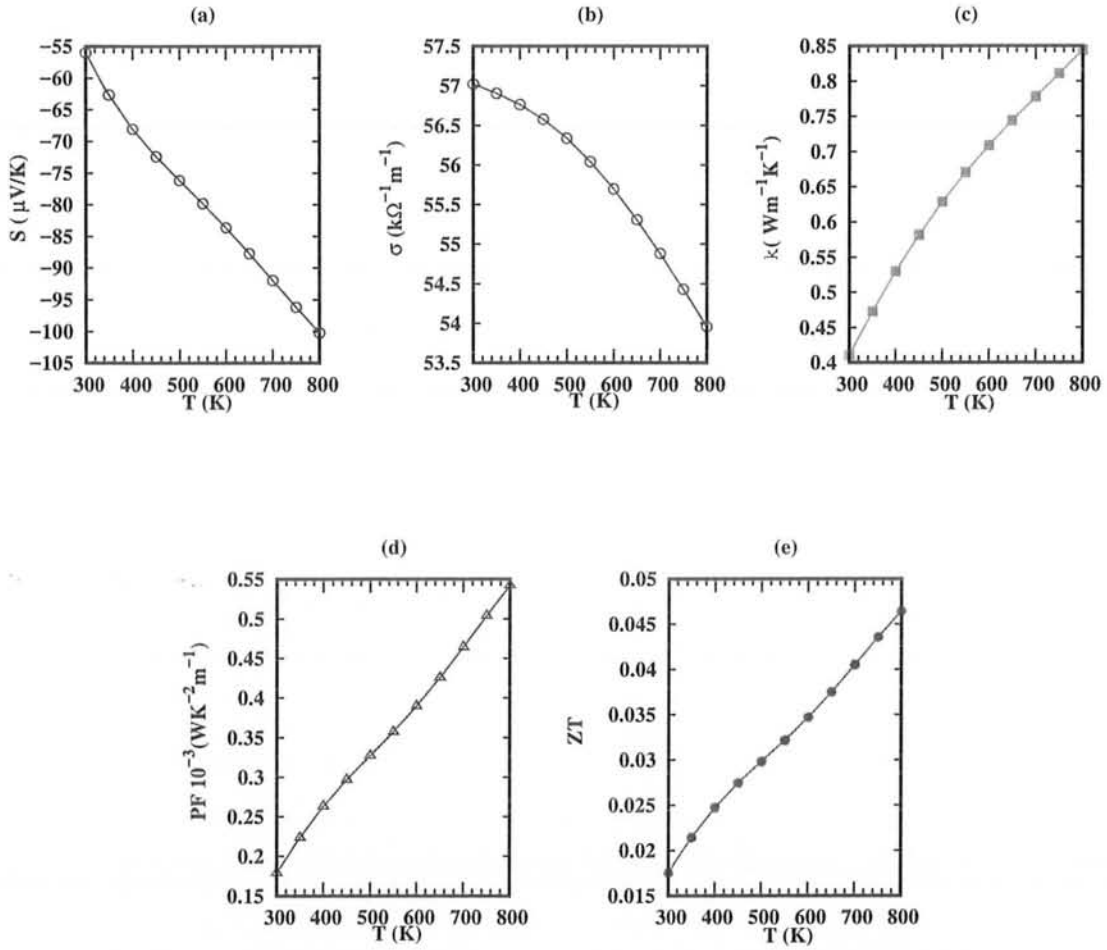

Figure 3.21: Thermoelectric parameters of System 04. (a), (b), (c), (d) and (e) represents thermopower, electrical conductivity, electron thermal conductivity, power factor and figure of merit respectively.

and reaches to 0.54 $10^{-3}(Wm^{-1}K^{-2})$ at 800K. While the value of figure of merit is 0.017 at 300K and reaches to 0.046 at 800K temperature. The calculated electronic band structure and DOS of Ta at Nb site $LiNbO_2$ indicates that it is very similar to pure $LiNbO_2$, both having a direct band gap with a small difference of 0.03 eV(2%). Ta and Nb both belongs to the same group in the periodic table, both having the same oxidation state (oxidation number). The only difference is the difference in the valence electron, which may be responsible for the small change in the band gap.

The thermoelectric transport properties of this system are calculated and shown in Fig. 3.22. Fig. 3.22[(a)-(e)] are Seebeck coefficient, electrical conductivity, thermal conductivity, power factor and figure of merit respectively.

The minimum value of Seebeck coefficient is 216 μV/K at 300K, and approaches to maximum value 237 μV/K at 600K. If we compare TE coefficient of this p-type System 05 with hole doped $LiNbO_2$, we can see that the minimum value of Seebeck coefficient of hole doped system at (1×10^{20} carrier concentration/cm^3) is 100 μV/K at 300K and reaches to 200 μV/K at 800K. The electrical conductivity of Ta at Nb is 2.6 (kS/m) at 300K, while 19 (kS/m) at 300K for hole doped $LiNbO_2$(1×10^{20} carrier concentration/cm^3). The minimum values of thermal conductivity, power factor and ZT for Ta at Nb site are, 0.05 ($Wm^{-1}K^{-1}$), 0.12 $10^{-3}(Wm^{-1}K^{-2}$ and 0.014, respectively at 300K temperature. Whereas the minimum values for hole doped system at (1×10^{20} carrier concentration/cm^3) are 0.2 ($Wm^{-1}K^{-1}$), 0.17 $10^{-3}(Wm^{-1}K^{-2}$ and 0.019, respectively at 300K. ZT of Ta at Li site and hole doped system become equal at (1×10^{20} carrier concentration/cm^3) at 800K temperature.

The band gap of Ni at Li site reduces to 1.43 eV, whereas it become more efficient among the doped systems. As the band gap decreases, results increase in the Seebeck coefficient and decrease in the thermal conductivity. The thermoelectric

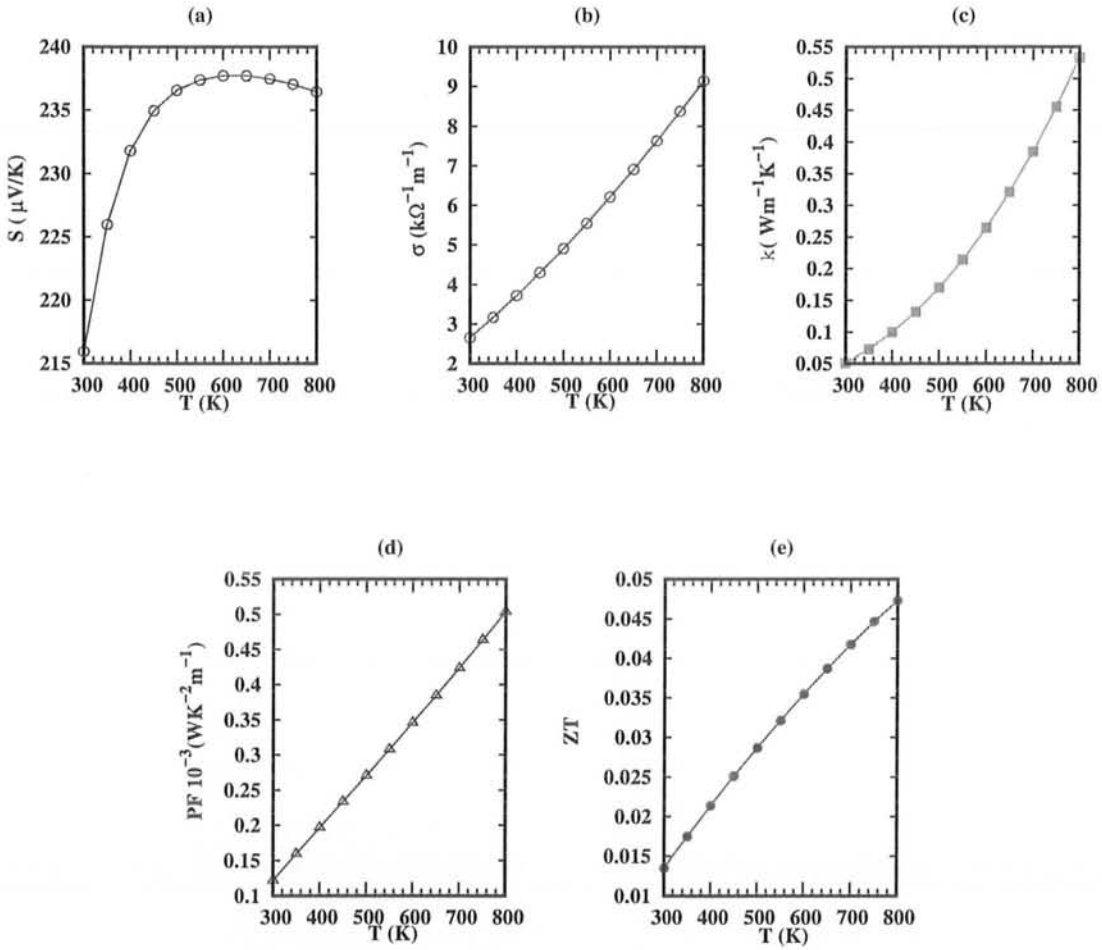

Figure 3.22: Thermoelectric parameters of System 05. (a), (b), (c), (d) and (e) represents thermopower, electrical conductivity, electron thermal conductivity, power factor and figure of merit respectively.

coefficients of this system are shown in Fig. 3.23. Fig. 3.23(a), Fig. 3.23(b), Fig. 3.23(c), Fig. 3.23(d) and Fig. 3.23(e) represents Seebeck coefficient, electrical conductivity, thermal conductivit, power factor and figure of merit, respectively. The minimum value of Seebeck coefficient is 60 μV/K at 300K and reaches to 260 μV/K at 600K temperature. The maximum value of electrical conductivity is 8.1 (kS/m) at 300K and reduce to 7.3 (kS/m) at 800K. Similarly the values of thermal conductivity, power factor and ZT at 300K are 0.055 ($Wm^{-1}K^{-1}$), 0.04 $10^{-3}(Wm^{-1}K^{-2})$ and 0.004, respectively. Maximum value of ZT is 0.057 at 600K.

The chemical potential near the Fermi level was used for calculating TE properties of these doped systems. All thermoelectric parameters at higher temperature are shown in table 3.4. The absolute value of thermopower is taken for System 04,

Table 3.4: Comparing T.E Parameters of doped Systems at 800K temperature.

System	S(μV/K)	σ(kS/m)	$\kappa_e(Wm^{-1}K^{-1})$	PF $10^{-3}(Wm^{-1}K^{-2})$	ZT
Sys 04	-100	53.95	0.843	0.541	0.046
Sys 05	236	8.97	0.532	0.501	0.047
Sys 06	250	8.07	0.118	0.46	0.0497

which is the minimum value in this table for Seebeck coefficient. Where maximum value of S is 250 μV/K for System 06. The electrical conductivity is maximum in System 04 (53.95 kS/m) and minimum in System 06(8.07 kS/m). Similarly the electron thermal conductivity is maximum in System 04 and minimum in System 06. Where the value of the figure of merit is quite different from these two Systems, e.g, 0.046 for System 04 and 0.0497 for System 06. The lattice thermal conductivity is also added to figure of merit. It shows that System 06 is more efficient from System

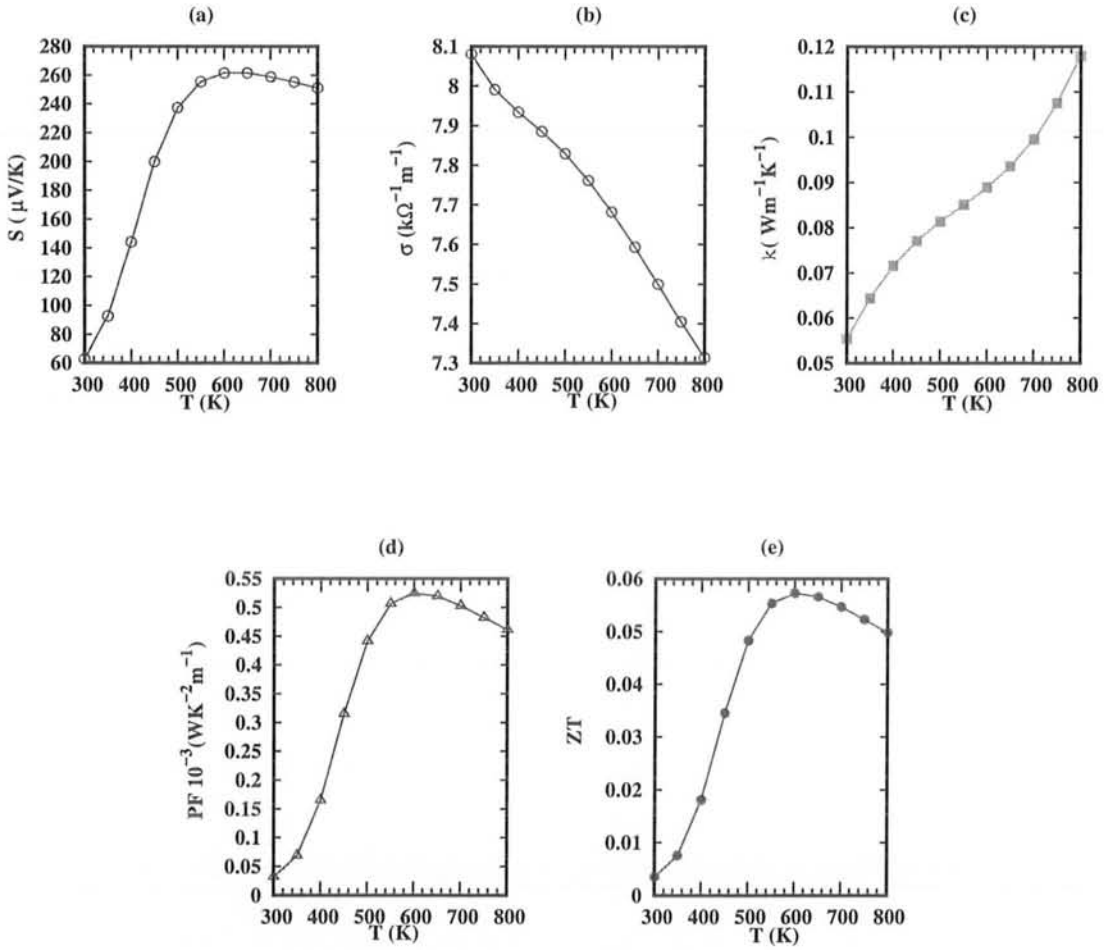

Figure 3.23: Thermoelectric parameters of System 06. (a), (b), (c), (d) and (e) represents thermopower, electrical conductivity, electron thermal conductivity, power factor and figure of merit, respectively.

04 and System 05, due to large thermopower and low thermal conductivity. One can further investigate this material for better TE performance.

Chapter 4

Conclusions

Using DFT with the help of BoltzTrap we find the thermoelectric properties of doped $LiNbO_2$. Calculations indicate that $LiNbO_2$ was found a direct band gap semiconductor. We first examine the thermoelectric properties of (electron and hole) doped $LiNbO_2$ as a function of carrier concentrations and temperature. In both cases the thermoelectric properties of electron doped were found better than hole doped system, due to the greater effective mass of the electron. The effective mass is directly related to Seebeck coefficient (Pisarenko's [10] relation) and so as its square is directly related to power factor.

The electronic and thermoelectric properties of Li vacancy and O vacancy were calculated. The band gap of these systems decreased, as a result the Seebeck coefficient was increased. The thermoelectric properties of these vacancy systems were calculated as a function of temperature. $LiNbO_2$ showed n-type behavior after O vacancy, and behaved p-type with Li vacancy. The efficiency of O vacancy was found better as compared with Li vacancy system.

Finally we doped $LiNbO_2$ with different atoms(Ta,Ni) at different sites. The for-

mation energy of these doped systems and vacancy system were calculated, which indicate that Ta doped at Nb site has the minimum formation energy. While Li vacancy system was found second stable system among them. TE properties were calculated for $Li_{1-x}A_xNbO_2$ (A=Ta,Ni), and $LiNb_{1-x}Ta_xO_2$ at (x=0.0625) as a function of temperature. Calculations indicate that $Li_{1-x}Ta_xNbO_2$ has better PF among these doped system, whereas the efficiency (ZT) of $Li_{1-x}Ni_xNbO_2$ was found better among them, due to large Seebeck coefficient and small thermal conductivity.

We observed that the electron doped $LiNbO_2$ as a function of carrier concentration/cm^3 has the highest TE performance among all combinations, whereas the calculated formation energy indicate that Ta at Nb site has the minimum formation energy, which is the most stable in these combinations. The TE properties of different systems in our calculations varies, so different changes can be made in $LiNbO_2$ to make it more efficient. Hence, we believe that Nb-doped $LiNbO_2$ could be a possible candidate material for thermoelectric applications. Our calculations also agree with the available experimental TE data of $LiNbO_2$.

Bibliography

[1] J. Goldsmid, *Introduction to Thermoelectricity*, Heidelberg, 3 (2009).

[2] B. Du, Han Li,C. Uher *Chem. of Mater.*, **22**, 5521 (2010).

[3] E. Velmre, *Biennial Baltic Elect. conf.*, 17 (2010).

[4] J. C. Peltier, *Ann. Chim. Phys.*, **1**, 371 (1834).

[5] B. Poudel, Q. Hao, Y. Ma, *A. A. for Adv. of sci.* **320**, 634 (2008).

[6] H. Li, X. Tang, Q. Zhang, *Appl. Phys. Lett.* **94**, 102114 (2009).

[7] K. Fujita, T. Mochida, K. Nakamura, *Jpn. J. Appl. Phys.* **40**, 4647 (2001).

[8] I. Terasaki, Y. Sasago, K. Uchinkura, *Phys. Rev. B*, **60**, 10584 (1999).

[9] D. M. Rowe, *CRC Handbook of Thermoelectrics*, CRC-Press, 44 (1995).

[10] A. F. Ioffe, *Physics of semiconductors*, New York, Academic Press, (1960).

[11] G. J. Snyder, E. S. Toberer, *Nat. Mat.*, **7**, 105 (2008).

[12] S. S. Li, *Semiconductor physical electronics*, Springer, Cha. 8 (2006).

[13] A. Sommerfeld, *Zur Elekt. der Met.*, **15**, 825 (1927).

[14] J. N. Reimers, J. R. Dahn, *J. Elect. Soc.*, **139**, 2091 (1992).

[15] N. Kumada, S. Muramatu, F. Muto, *J. S. S. Chem.*, **73**, 33 (1988).

[16] G. Meyer, R.Hoppe, *Ange. Chem.*, **86**, 819 (1974).

[17] D. L. Novikov, V. G. Zubkov, *Phys. Rev. B* , **49**, 15830 (1994).

[18] M. J. Geselbracht, A. M. Stacy, *J. Phys. Chem.* **97**, 7102 (1993).

[19] E. G. Moshopoulou, P. Bordet, *Phys. Rev. B*, **59**, 9590 (1999).

[20] J. Rahman, E.J. Meaning, *J. Electron . Mater.* **46**, 1740 (2017).

[21] E. Schrödinger, *A. d. phy.*, **385**, 437 (1926).

[22] J. Thijssen, *Computational physics*, Cambridge, 44 (2007).

[23] P. Hohenberg, W. Kohn, *Phys. Rev.* **136**, 865 (1964).

[24] J. J. Sakurai, J. Napolitano, *Modern quantum mechanics*, Addison Wesley, 332 (2011).

[25] W. Kohn and L. J. Sham. *Phys. Rev.*, **140**, 1133 (1965).

[26] J. P. Perdew, A. Zunger ,*Phys. Rev. B*, **23**, 5048 (1981).

[27] J. Heyd, G. E. Scuseria, *J. Chem. Phys.* **118**, 8207 (2003).

[28] A. D. Becke, *J. Chem. Phys.*, **98**, 1372 (1993).

[29] R.G. Parr, W. Yang, *Q. chem.*, **47**, 101 (1993).

[30] J. P. Perdew , A. Zunger. *Q. Chem.*, **23**, 101 (1993).

[31] C. Herring, *Phys. Rev.*, **57**, 1169 (1940).

[32] D. R. Hamann *Phys. Rev. B.*, **88**, 85117 (2013).